Hydrologic behavior of model slopes with synthetic water repellent soils

Shuang Zheng[1], Sérgio D.N. Lourenço[1*], Peter J. Cleall[2], Ting Fong May Chui[1], Angel K.Y. Ng[3], Stuart W. Millis[3]

[1] Department of Civil Engineering, The University of Hong Kong, Hong Kong S.A.R., China

[2] School of Engineering, Cardiff University, United Kingdom

[3] Ove Arup & Partners (Hong Kong) Ltd., Hong Kong S.A.R, China

* Corresponding author

Abstract

In the natural environment, soil water repellency decreases infiltration, increases runoff, and increases erosion in slopes. In the built environment, soil water repellency offers the opportunity to develop granular materials with controllable wettability for slope stabilization. In this paper, the influence of soil water repellency on the hydrological response of slopes is investigated. Twenty-four flume tests were carried out in model slopes under artificial rainfall; soils with various wettability levels were tested, including wettable (Contact angle, CA <90°), subcritical water repellent (CA ~90°) and water repellent (CA >90°). Various rainfall intensities (30 mm/h and 70 mm/h), slope angles (20° and 40°) and relative compactions (70% and 90%) were applied to model the response of natural and man-made slopes to rainfall. To

quantitatively assess the hydrological response, a number of measurements were made: runoff rate, effective rainfall rate, time to ponding, time to steady state, runoff acceleration, total water storage and wetting front rate. Overall, an increase in soil water repellency reduces infiltration and shortens the time for runoff generation, with the effects amplified for high rainfall intensity. Comparatively, the slope angle and relative compaction had only minor contribution to the slope hydrology. The subcritical water repellent soils sustained infiltration for longer than both the wettable and water repellent soils, which presents an added advantage if they are to be used in the built environment as barriers. This study revealed substantial impacts of man-made or synthetically induced soil water repellency on the hydrological behavior of model slopes in controlled conditions. The results shed light on our understanding of hydrological processes in environments where the occurrence of natural soil water repellency is likely, such as slopes subjected to wildfires and in agricultural and forested slopes.

Keywords: Soil wettability, synthetic water repellent soil, hydrological behavior, flume test

1. Introduction

Wildfire-induced water repellent soil (soil that exhibit low affinity for water) is widely known for altering the hydrological responses and vadose zone processes of hillslopes, such as formation of unstable wetting front and fingered flow (preferential flow), restricted soil water movement and redistribution, decreased infiltration rate and promoted surface runoff (Doerr et al., 2006; Ritsema and Dekker, 2000; DeBano, 2000). By impeding infiltration into soil matrix, enhancing the overland flow and increasing the erodibility of soils, the likelihood of post-wildfire debris flows and consequent flash floods is increased (Fox et al., 2007; Cannon et al., 2008; Kean et al., 2012; Robichaud et al., 2016).

Soil wettability, a measure of the affinity of soils for water, is closely related to the stability of slopes. The strong correlation between post-wildfire debris flows and the formation or enhancement of soil water repellency has been extensively reported. Soil water repellency reduces the infiltration rate and increases the erodibility thereby resulting in increased overland flow and erosion. On the other hand, for wettable natural soils (soils that exhibit high affinity for water) the infiltration rate is relatively high and rainwater is able to infiltrate through the slope and form a saturated zone above any impermeable layer, leading to a rapid rise in the pore water pressure and a decrease of the effective stress and soil strength eventually triggering failure (Wang and Sassa, 2001; Tohari et al., 2007) whilst other factors known to influence slope stability of wettable soils such as rainfall intensity (RI), slope angle and relative compaction (for man-made slopes) have been widely reported and known for

60 decades, little is known about their effects with regard to water repellent soils in slopes.

61

62 The soil-hydraulic properties of burned and unburned soils have been measured and
63 compared). Ebel and Moody (2017) reported that the mean value of sorptivity (a measure of
64 the liquid movement in a porous material by capillarity) for unburned soils was seven times
65 greater than that of burned soils, whereas the field saturated hydraulic conductivity was not
66 significantly decreased in burned soils compared with unaffected soils. However, Fox et al.
67 (2007) and Robichaud (2000) conducted laboratory and field experiments and observed
68 reduced saturated hydraulic conductivity on water repellent soils. The effects of water
69 repellency on other soil properties have also been investigated, such as water retention
70 (Czachor et al., 2010; Lourenço et al., 2015a), splash erodibility (Ahn et al., 2013), water drop
71 impact (Hamlett et al., 2013), and permeability and compressibility for saturated wax-coated
72 soils (Bardet et al., 2014), water entry pressure and friction angle (Lee et al., 2015) and
73 small-strain shear modulus (Choi et al., 2016). However, although the association between
74 wildfire-induced water repellency and enhanced hydrological response in the form of runoff
75 and erosion is generally accepted, it is challenging to separate the influence of water
76 repellency from other impacts such as a reduction in the vegetation cover and surface sealing
77 with pore clogging.

78

79 Although soil water repellency is generally linked to limited or no infiltration, debris flows and
80 erosion, its ability to impede water infiltration into soil has drawn the interest of engineers due
81 to its waterproof capabilities. Synthetic water repellent soils have been used for water

82 harvesting in arid areas (Meyers and Frasier, 1969). DeBano (1981) proposed the installation
83 of a water repellent layer in the pavement base to prevent water permeation and protect the
84 pavement from freezing and thawing. The potential use of synthetic water repellent soils as
85 alternative landfill cover has also been proposed by Dell'Avanzi et al. (2010). Lourenço et al.
86 (2015c) conducted a series of flume tests to model the response of slopes under rainfall, by
87 manipulating the level of wettability from wettable to water repellent to explore the application
88 of water repellent soils in slope engineering. Bardet et al. (2014) applied wax-coated sands
89 on horseracing tracks and sports fields to avoid the degradation of the soil properties under
90 rainfall.
91
92 To date, the use of synthetic water repellent soils has only considered a fully water repellent
93 condition where no infiltration occurs (impermeable to water). However, wettability is
94 controllable with the possibility of adjusting its condition so that some water infiltrates (i.e.
95 semi-permeable to water). This could represent an added advantage for applications where
96 vegetation is required to grow or where erosion is expected. Therefore, since extreme
97 wettability conditions can cause slope instability in the form of landslides or erosion, the
98 optimal conditions that reduce or inhibit slope instability need to be established so that
99 synthetic water repellent soils could be deployed on sloping ground. This paper explores the
100 influence of four factors assumed to alter the hydrologic response of the slope, namely: level
101 of water repellency, slope angle, soil relative density and rainfall intensity.
102
103 The aim of the paper is to investigate the effect of synthetically induced soil water repellency

104 on the hydrological response of slopes with a view to establish the conditions that minimize
105 slope instability, either through excessive runoff, erosion or slope failure. In particular, soils
106 with three wettability levels (wettable, subcritical water repellent and water repellent) were
107 tested through a series of flume tests in model slopes at defined relative compactions, slope
108 angles and rainfall intensities. The wettability levels are based on the contact angle (CA). If
109 the water drop is placed on a water repellent surface, it does not infiltrate instantaneously.
110 The angle that develops at the three-phase line is called the CA, which depends on the
111 relation between the interfacial energies of the three involved surfaces (solid, liquid and
112 vapor). The CA of a wettable soil and water repellent soil is <90° and >90° respectively, and a
113 subcritical water repellent soil has a CA ~90°. A subcritical water-repellent condition reduces
114 infiltration and is generally regarded as a wettability boundary between wettable and water
115 repellent soil (Czachor et al., 2010). The specific objectives of the study are: 1) to identify the
116 infiltration modes and estimate the infiltration rates for the different wettability levels; 2) to
117 assess the longevity of the wettability levels (for the sub-critical and water repellent soils); 3)
118 to assess the effects of rainfall intensity, slope angle and relative compaction on the
119 hydrological responses within each wettability level; and 4) to determine the optimal
120 conditions under which the runoff, erosion or slope failure is diminished or inhibited.
121

122 **2. Materials and Methods**

123

124 *2.1. Soil description*

125

126 The soil selected in this study is completely decomposed granite (CDG), collected from
127 Happy Valley, Hong Kong, which is widespread locally and commonly used as an engineering
128 soil and fill material (Lumb, 1965). The mineralogy of CDG was analyzed using X-ray
129 diffraction (XRD) (Philips, PW1710 Automated Powder Diffractometer, Almelo, The
130 Netherlands), and the major mineral compositions are quartz and kaolinite. Particle size
131 distribution, compaction behavior and organic matter content were obtained for the natural
132 CDG (Table 1). The percentage of sand and fines was 49.47% and 34.47% respectively. The
133 high proportion of fines agrees with the large proportion of kaolinite from the XRD results. The
134 CDG is classified as a well-graded silty sand based on the particle size distribution (Figure 1).
135 The maximum dry density and optimum water content with the light Proctor test were 1.57
136 Mg/m^3 and 23%, respectively. Loss on ignition (LOI) analysis was conducted to determine the
137 organic matter content (BS 1377-3:1990). Sub-samples were heated at 450°C for 1 hour. The
138 organic content was 1.95%. The soil was air-dried and sieved (6.30 mm mesh with the
139 coarser material discarded) for further use.
140
141 *2.2. Soil water repellency assessment*
142
143 Two measuring techniques were adopted in this study to assess the level of water repellency
144 of different soil samples: the sessile drop method (SDM) and water drop penetration time
145 (WDPT).
146

147 2.2.1. Sessile Drop Method

148

149 The SDM is a direct method to measure the CA of water drop on a soil sample surface. This
150 method was improved by Bachmann et al. (2000) and the procedure is as follows: the soil is
151 sprinkled on a double-sided adhesive tape fixed on a glass slide, the excess particles are
152 removed to ensure a monolayer of particles is fixed and any motion of the particles is
153 prevented. Placing the slide on a goniometer's stage and dispensing a droplet of deionized
154 water (10μL) on the sample. CA measurements are then performed with a goniometer (DSA
155 25, KRÜSS GmbH, Germany), by analyzing the shape of the droplet on the soil surface. The
156 analyzing technique proposed by Saulick et al. (2017) was adopted. By applying this
157 semi-automatic technique, the standard deviation of measurements on a granular surface
158 was improved by 33%, comparing to the conventional analyzing technique.

159

160 2.2.2. Water Drop Penetration Time test

161

162 WDPT is an index test that evaluates the persistency of water repellency of a soil sample.
163 The test involves dispensing a drop of deionized water (50μL) on the surface of prepared soil
164 sample and recording the time for the water drop to completely infiltrate (Doerr, 1998). For
165 wettable soils the water drop should penetrate immediately, and for water repellent soils, the
166 stronger the water repellency the longer the time it takes to fully infiltrate. Based on the
167 penetration time, the water repellency of soils can be classified into different categories
168 (Table 2).

169

170 *2.3. Water repellent soil treatment*

171

172 Inorganic soils are considered to be wettable as the surface energy of commonly composing
173 minerals (silica and calcite) is higher than that of water (Lourenço et al., 2015b). The
174 occurrence of soil water repellency results from the presence of water repellent coatings
175 around the soil particles. Naturally occurring soil water repellency is usually caused by plant
176 surface wax and certain fungi species (Bisdom et al., 1993; DeBano, 2000). Therefore, a
177 variety of water repellent substances similar to those in nature has been used to induce water
178 repellency, such as stearic acid (Leelamanie and Karube, 2009), oleic acid (Wijewardana et
179 al., 2015) and tung oil (Zhang et al., 2016).

180

181 Natural soil water repellency is not time-stable, with changes in the wettability status possible
182 with time. To achieve persistent and stable soil water repellency, dimethyldichlorosilane
183 (DMDCS) has been used as a hydrophobizing agent to form a water repellent coating on soil
184 samples (Bachmann et al., 2000; Ng and Lourenço, 2016). The mechanism of the treatment
185 is based on silanization. By reaction between DMDCS and residual water,
186 polydimethylsiloxane (PDMS) is formed and bonded to the soil particle surface along with the
187 formation of HCl gas as a by-product.

188

189 The level of water repellency depends on the concentration of DMDCS and soil type.
190 Bachmann et al. (2000) used 7.5 mL DMDCS per kg of sand and 50 mL DMDCS per kg of silt

191 to attain a CA~90° (which is a quantification of water repellency). Ng and Lourenço (2016)
192 found that the maximum CA can be induced by 3% and 0.005% DMDCS by soil mass for
193 alluvium and Leighton Buzzard sand, respectively. The concentration of DMDCS to attain
194 high water repellency in CDG was found to be 3% DMDCS by soil mass to achieve a CA
195 ~115° (Figure 2). After the treatment, a significant increase in the level of soil water repellency
196 was observed. As shown in Figure 3, the CAs of treated soils increased in the first 3 days and
197 then slightly fluctuated, regardless of the DMDCS concentration. This was assumed to be
198 due to a continuing reaction with water vapor to release the hydrochloric acid. To allow water
199 repellency to establish in the soils and for consistency among the tests, the soil was treated
200 and equilibrated at ambient air conditions for 3 days before using.
201
202 *2.4. Flume tests*
203
204 Flume tests at various scales have been widely conducted to study the initiation and
205 dynamics of debris flows under artificial rainfall (Eckersley, 1990; Iverson and LaHusen, 1993;
206 Wang and Sassa, 2001; Lourenço et al., 2015c). To investigate the influence of wettability
207 change on hydrological responses of soil, 24 flume tests were carried out in a perspex-sided
208 flume. The dimensions of the physical model were 80 cm long, 40 cm wide and 10 cm high.
209 Sandpaper (Simax LPE-22-4) was glued on the bottom of the flume to provide friction and
210 prevent the model from sliding at the flume-soil interface. As this research focuses on the
211 hydrological response of soils of variable wettability under rainfall and to minimize potential
212 mechanical effects, a baffle was installed at the toe of the slope to prevent sliding of the soil

213 mass. The absence of a retaining element at the toe of the slope would enhance erosion in
214 the toe area. This was the case in flume tests with a trapezoidal shape (Lourenço et al., 2006)
215 where toe erosion and back-sliding controlled failure. Artificial rainfall was generated by a
216 nozzle, controlled by a flowmeter, to ensure constant RI during tests. Four capacitance
217 moisture sensors (EC-5, Decagon Devices, US) were installed at two different depths (3 and
218 8 cm respectively) to track the volumetric water content change. The sensors measure the
219 volumetric water content of the soil by measuring the dielectric permittivity, and a soil-specific
220 calibration was performed using the technique recommended by Cobos and Chambers
221 (2010). A video camera (HERO4 Silver, GoPro, US) was positioned parallel to the side to
222 capture the movement of the wetting front and the slope failure process. The resolution of the
223 camera is 3840 × 2160 pixels with a sampling frequency of 15 frames per second. Figure 4
224 shows the configuration of the flume and instrumentation.
225
226 2.4.1. Model preparation and test procedure
227
228 Testing was conducted on dry water repellent CDG since water repellency develops in drier
229 soils. The CDG was initially air-dried and treated to the desired CA, no water was added and
230 no oven-drying was conducted prior or after treatment as the temperature is known to
231 influence soil water repellency. The model was compacted in a horizontal orientation into 10
232 layers with a thickness of 1 cm. For each layer, the mass of soil was calculated and the
233 dumping height and compaction energy controlled to attain a given relative compaction. Four
234 moisture sensors were buried during the compaction, two on the second layer (depth: 8 cm)

235 and the other two on the seventh layer from the bottom (depth: 3 cm). In order to prevent
236 infiltration on the flume sides, a side wall intercept was glued on both sides of the flume to
237 divert the rainfall out of the flume (Figure 4a). This portion of the rainfall was collected
238 together with the surface runoff and excluded in the data analysis. After compaction, the
239 flume was inclined to the desired slope angle.
240
241 At the onset of each test, the artificial rainfall was applied at a determined intensity. The
242 advance of the wetting front, which was sensitive to the wettability change, was monitored by
243 the camera. This information was validated by the moisture sensors, which can trace the
244 spatial evolution of wetting at 1-minute intervals. Runoff and the soil discharge were collected
245 by a storage container at the end of the flume at 5-minute intervals. Runoff is equivalent to
246 the difference between rainfall intensity and effective rainfall rate. When the steady state is
247 reached, the runoff discharge equals to rainfall intensity and remains unchanged, that means
248 the effective rainfall is zero. Within this context, the term runoff does not necessarily imply
249 overland flow. As will be later presented, most observed runoff occurs at the sub-surface, with
250 water flowing within the top mm's of the soil profile parallel to the surface.
251
252 2.4.2. Testing programme
253
254 Twenty-four flume tests were conducted (Table 3) under different slope inclinations, relative
255 compactions, rainfall intensities and wettability. As this study originates in Hong Kong, the
256 slope angles, relative compactions and rainfall intensities were selected to represent Hong

257 Kong natural and man-made slopes. Slope inclinations were from 20° to 40°, where 20° is on
258 the small end of slope angle for local man-made slopes (Sun, 1999) and 40° is the largest
259 that can be obtained using this flume. The majority of fill slopes in Hong Kong are within this
260 range. The two relative compactions selected were 70% and 90%, with a corresponding dry
261 density of 1.10 Mg/m^3 and 1.41 Mg/m^3, respectively. For the relative compaction, 70%
262 corresponds to an uncompacted soil, whilst 90% is the maximum relative compaction that
263 can be obtained with the soil in a dry state.
264
265 As for RI, black and amber rainstorm signals of Hong Kong's rainstorm warning system (Li
266 and Lai, 2004) were selected with the intensities of 70 mm/h and 30 mm/h respectively. The
267 Hong Kong Intensity-Duration-Frequency (IDF) relationships recommended in the stormwater
268 drainage manual (Drainage Services Department, 2013) was adopted to determine the
269 relation between rainfall duration, rainfall intensity and the return period. A rainfall duration of
270 120 minutes was adopted for all tests, since preliminary testing indicated that the steady state
271 condition was achieved for the duration of 90-120 minutes. Therefore, a rainfall duration of
272 120 minutes under a RI of 70 mm/h and 30 mm/h correspond to a return period of 10 years
273 and 2 years, respectively. There was a small difference in the RI among the tests at 20° and
274 40° slope angles, as the nozzle was fixed in vertical orientation and the area of apparent
275 horizontal plan changes with slope angle. The RI was determined by measuring the volume
276 of rainfall that accumulated in cups at various locations. The actual RI was 69.8±6.1 mm/h
277 and 30.4±1.8 mm/h for a slope angle of 40°, and 74.4±4.6 mm/h and 34.2±3.3 mm/h for a
278 slope angle of 20°.

279

280 Three water repellency levels were selected by treating the CDG at increasing concentrations
281 of DMDCS. The criteria were based on the CA and WDPT attained. For a wettable condition
282 the CA and WDPT should be as low as possible. For a sub-critical water repellent condition
283 the CA should be ~90° and the WDPT >0 seconds. For a water repellent condition the CA
284 and WDPT should be as high as possible. Therefore, the CDG in an untreated state delivered
285 a CA ~55° and a WDPT = 0 seconds corresponding to the wettable condition. Sub-critical
286 water repellent conditions were achieved at 1.8% DMDCS concentration (CA ~92°, WDPT
287 rising). Water repellent conditions were achieved for 3% DMDCS concentration (CA ~115°,
288 WDPT extreme) (Figure 2).

289

290 *2.5. Data analysis*

291

292 The raw data generated in each test includes: 1) volumetric water content at 4 different
293 locations; 2) runoff discharge at 5-minute intervals and 3) photographs of infiltration modes. A
294 series of variables were defined to analyze the data (Figure 5):

295

296 • Runoff rate (q, mm/h): Volume of water runoff collected at each 5-minute interval.

297

298 • Effective rainfall rate (i, mm/h): Difference between RI (r, mm/h) and runoff rate (q) at
299 each 5-minute interval (Stoof et al., 2014). Both the runoff rate (q) and effective rainfall
300 rate (i) were presented in time series. The expression for infiltrate rate is as follows:

$$i = r - q \quad (1)$$

- Time to ponding (t_p, min): Determined from visual inspection of ponding at the slope surface (Diskin and Nazimov, 1996) and a corresponding growth in the runoff rate (q).

- Time to steady state (t_{ss}, min): Time at which the runoff rate (q) is equal to the rainfall intensity. The time to steady state (t_{ss}) follows the time to ponding (t_p) and corresponds the time at which all rainfall becomes runoff (i.e. no more water storage).

- Runoff acceleration (a_q, mm/h^2): The temporal change in the runoff rate (q) (not the temporal change in water flow velocity) from time to ponding (t_p) to time to steady state (t_{ss}). It represents how fast the runoff developed before steady state was reached and can be calculated by

$$a_q = \frac{\Delta q}{t_{ss} - t_p} \quad (2)$$

- Total water storage (S, mm): Cumulative effective rainfall rate during the 120 minutes rainfall event, which equals the difference between total rainfall and total runoff.

$$I = \sum_{t=0}^{120} it = \sum_{t=0}^{120} rt - \sum_{t=0}^{120} qt \quad (3)$$

- Wetting front rate (v_{wf}, mm/min): The distance between moisture sensors 1 and 3 (or 2 and 4) (50 mm) divided by the time taken to travel from one to the other. The wetting front rate evaluates how fast the wetting front moved downward. The photographs from the side of flume were converted to black and white in order to show the infiltration modes. Six times were selected for each test to represent the evolution of the wetting fronts.

$$V_{wf} = \frac{50}{\Delta t} \quad (4)$$

The hydrological responses of the treated and untreated soils were sensitive to wettability changes, and thus the tests were analyzed in 3 categories according to the wettability, i.e. wettable soil, subcritical water repellent soil and water repellent soil. The effects of soil water repellency were compared among categories, while the influences of slope angle, RI and relative compaction were studied within each level. One representative test was selected from each group and presented in time series to describe the typical responses. The volumetric water content change, runoff and effective rainfall data are shown in Figure 6 to Figure 8, and the infiltration modes are summarized in Figure 9.

Statistical analysis is also conducted, the normality and homogeneity of all variables are verified using the Lilliefors test and Bartlett test, respectively. When the assumptions are satisfied, the parametric test (balanced one-way ANOVA) is used. If the null hypothesis is rejected, the non-parametric test (Kruskal-Wallis test) (Kruskal and Wallis, 1952) is then

adopted.

3. Results

3.1. Calibration of moisture sensor

Soil-specific calibrations were conducted for wettable and subcritical water repellent soils, with the calibration equations presented in Figure 10. Calibration was not performed for the water repellent soil as infiltration did not occur. The calibration equation obtained for the wettable soil was $VWC = 9 \times 10^{-4} \times raw - 0.4537$, where VWC is the volumetric water content, and was different from the calibration equation provided by the manufacturer ($VWC = 8.5 \times 10^{-4} \times raw - 0.48$), which consistently provided lower volumetric water contents. The calibration equation for the subcritical water repellent soil was $VWC = 4 \times 10^{-4} \times raw - 0.2156$, suggesting that this relation is considerably affected by the DMDCS treatment. However, the calibration equation for the wettable soil was used for all tests, as will be discussed later.

3.2. Statistical analysis

The statistical significance analysis on the impacts of RI, slope angle, relative compaction and initial wettability are summarized in Table 4. The sample sizes, mean values, standard deviations and p-values (significance level = 0.05) are presented. From the analysis, the impacts of relative compaction and slope angle on all five measurements are not statistically

367 significant. As for the effects of RI, time to ponding, time to steady state, wetting front rate and
368 total water storage show statistical non-significance, whereas a strong correlation is observed
369 between RI and runoff acceleration. The effect of the initial wettability on the hydrological
370 responses is verified, as the results of various wettability are of different statistical
371 significance.
372
373 The effects of RI, slope angle, relative compaction and initial wettability on hydrological
374 responses are presented in Figure 11. Results of all tests are summarized together, box and
375 whisker plots are adopted to establish comparisons among the data sets. In the plot, the ends
376 of the box are the upper and lower quartiles, the median is marked by a solid line inside the
377 box, and the mean is marked by a cross inside the box, the whiskers are the two lines outside
378 the box that extend to the highest and lowest values observed.
379
380 *3.3. Wettable soils*
381
382 The results of representative wettable soil are shown in Figure 6 (test 1). The runoff rate and
383 effective rainfall rate are presented in Figure 6a, the change in volumetric water content at
384 several locations are recorded once a minute in Figure 6b, the infiltration mode is presented
385 in Figure 9a. An expanding wetted zone at the slope toe was observed which was caused by
386 the accumulation of water near the baffle. The remaining part of the slope was not affected.
387 Figure 9a shows a wetting front parallel to the slope surface and moving downward gradually,
388 this observation agreed with the results of volumetric water content change (Figure 6b) with

389 the readings of sensor 1 and 2 unchanged at the beginning and suddenly rising at 7 minutes
390 simultaneously. At 22 minutes, the same responses occurred for sensors 3 and 4. The time
391 difference between sensors 1 and 2, and sensors 3 and 4 was 15 minutes. During infiltration,
392 the volumetric water content kept increasing until 47.2% for moisture sensors 1 and 2. This
393 implies the soil was nearly saturated, since for the soils at 70% and 90% relative compaction,
394 the volumetric water content at saturation should be 55.4% and 46.8%, respectively. The
395 difference among moisture sensors (around 8% for sensors 1 and 2 and 3 and 4) (Figure 6b)
396 could be due to the density increase with depth, as higher relative compaction leads to a
397 lower volumetric water content at saturation.
398
399 The hydrological response of the wettable soils followed a three-stage sequence, regardless
400 of the slope angle, RI and relative compaction (Figure 6a). In the first 15 minutes all rainfall
401 infiltrated and no surface runoff was observed, implying that the RI was smaller than the initial
402 infiltration capacity, which is the maximum rate at which water can infiltrate into a given soil.
403 From 15 minutes to 65 minutes, the effective rainfall rate started to decrease together with a
404 concomitant increase in runoff rate. At 65 minutes, a steady state was reached with the
405 effective rainfall rate reduced to zero and the runoff rate equal to the RI i.e. all rainfall was
406 converted to runoff.
407
408 The mean time to ponding (t_p) and mean time to steady state (t_{ss}) do not show much
409 differences. The mean runoff acceleration (a_q) shows that high RI leads to high runoff
410 acceleration (126.7 mm/h^2), comparing to 64.6 mm/h^2 at low RI (Figure 11c). The mean

411 wetting front rate (v_{wf}) shows that the wetting front traveled faster under high RI (2.9 mm/min)
412 than under low RI (1.8 mm/min) (Figure 11d). The total water storage (S) results suggest an
413 influence of the slope angle with the steeper slopes allowing a lower total water storage (38.4
414 mm) than the gentler slopes (42.6 mm) (Figure 11e).
415
416 *3.4. Subcritical water repellent soils*
417
418 The results of representative subcritical water repellent soil are shown in Figure 7 (test 8).
419 The runoff rate and effective rainfall rate are presented in Figure 7a, change in volumetric
420 water content at several locations are recorded in Figure 7b, the infiltration mode is presented
421 in Figure 9b (The other infiltration mode of subcritical water repellent soil is shown in Figure
422 9c and discussed later). Infiltration still occurred in the subcritical water repellent soil,
423 although the wetting front rate was significantly reduced. This observation agreed with the
424 result of the volumetric water content change (Figure 7b), with the readings of sensors 1 and
425 2 unchanged at the start of the test and rising at around 10 minutes. At 80 minutes, the
426 volumetric water content in sensors 3 and 4 started to increase. The time difference between
427 sensors 3 and 4, and sensors 1 and 2 was around 70 minutes, which is longer than the
428 difference for the wettable soil (around 15 minutes). As for the infiltration mode, unlike the
429 wettable soil whose wetting front was parallel to the slope surface, preferential flow (fingering)
430 and horizontal percolation were observed in subcritical water repellent soil. Along with the
431 evolution of infiltration, the volumetric water content kept increasing until the maximum was
432 reached. For the subcritical water repellent soil, the reading of the sensors was very high at

59.7%, as the volumetric water content of the saturated soil is only 46.8%. However, the time at which the sensor measured the increase in the volumetric water content was accurate and was used to calculate the wetting front rate. The calibration equation for the subcritical water repellent soil was not adopted to acquire water content data. Because the influence of DMDCS treatment gradually reduced with the draining of subsurface flow, the calibration equation of the subcritical water repellent soil could change with time. Therefore, the calibration equation for the wettable soil was used for all tests.

The hydrological response of the sub-critical water repellent soils also followed a three-stage sequence, regardless of the slope angle, RI and relative compaction (Figure 7a). Runoff was observed from 0 minutes (when the rainfall started), implying that the initial infiltration capacity after treatment is reduced and less than the RI. The runoff rate increased from 0 to 20 minutes. From 20 to 65 minutes, the runoff rate increased albeit with a smaller runoff acceleration (around 15% of the first stage). From 65 minutes, a steady state was reached with the effective rainfall rate reduced to zero and the runoff rate equal to the RI i.e. all rainfall was converted to runoff.

The mean time to ponding and mean time to steady state have similar magnitudes. The runoff acceleration showed that high RI leads to high runoff acceleration (67.6 mm/h^2), comparing to 28.2 mm/h^2 at low RI (Figure 11c). The wetting front rate varied considerably for both high RI (0.5-1.5 mm/min) and low RI (0-1.4 mm/min) (Figure 11d), and the variation is less than that of wettable soil, indicating that the influence of RI on wetting front rate was not

455 as significant as soil water repellency. The total water storage, showed that at a high slope
456 angle the mean total water storage is slightly less (16.9 mm) than that of a low slope angle
457 (31.6 mm), suggesting that there is less water storage in steeper slopes (Figure 11e).
458
459 *3.5. Water repellent soils*
460
461 The results of representative water repellent soil are shown in Figure 8 (test 15). The runoff
462 rate and effective rainfall rate are presented in Figure 8a, the change in the volumetric water
463 content at several locations are recorded in Figure 8b, the infiltration mode is presented in
464 Figure 9d. Infiltration was prevented by the soil water repellency for all the tests, with only a
465 thin layer at the millimeter scale of the slope surface wetted. The wetting front rate was not
466 calculated as no infiltration was observed. This observation agreed with the volumetric water
467 content data (Figure 8b), with the sensors readings unchanged for all tests.
468
469 Runoff was observed from 0 minutes with no infiltration occurring. However, sub-surface flow
470 parallels to the surface were noted in the upper 2-3 mm with water flowing to the bottom of
471 the model and wetting the baffle area. These observations differed from those of Lourenço et
472 al. (2015c) where industrial silica sand was used and runoff, erosion and rills developed on
473 the model surface. This difference could be linked to the differences in the particle size and
474 mineralogy, the erodibility of cohesionless clean sand is much greater than completely
475 decomposed granite, whose clay fraction provides sufficient cohesion to prevent erosion in
476 the current study. As such, the erosion and rills were observed only with silica sand.

Only two stages in the runoff generation process were identified in Figure 8a, runoff rate increased up to a steady state condition. The runoff rate started to increase at the start of the test, until the steady state was reached at 30 minutes. After which a steady state was reached with the effective rainfall rate reduced to zero and the runoff rate equal to the RI i.e. all rainfall was converted to runoff.

There is no significant difference observed between the mean time to ponding and mean time to steady state. The runoff acceleration shows variable runoff acceleration for high RI (101.4-332.4 mm/h^2) and low RI (33.9-342 mm/h^2) (Figure 11c), implying that the water repellent condition of the soil dominates runoff regardless of the RI. The wetting front rate cannot be determined by Eq. (4) since no water reached the sensors (Figure 11d). According to the visual observation and runoff data, no infiltration was allowed and therefore the wetting front rate was 0. The total water storage showed that at a high slope angle the mean total water storage is slightly less (6.4 mm) than that of a low slope angle (12.9 mm), suggesting that less water can be stored in steeper slopes (Figure 11e). However, the total water storage should be 0 mm. Sources of infiltration include (1) subsurface flow at the uppermost 2-3 mm depth of the soil and, (2) infiltration near the baffle area due to the accumulation of water from the subsurface flow and the wettable nature of the baffle (acting as a preferential infiltration interface) (Figure 12).

4. Discussion

4.1. Effect of initial soil wettability

The initial wettability condition had a profound effect on the hydrological response of the soils, as shown by the statistical analysis. All tests are summarized and compared to examine the influence of the initial wettability condition on the runoff hydrograph, wetting front rate, total water storage, time to ponding, time to steady state and runoff acceleration.

The runoff hydrographs of the soils (*i.e.* the shape of the runoff/effective rainfall rate in Figures 6a, 7a and 8a) are shown in Figure 13. Since the RI and runoff rate of each test differs, the RIs for all tests are normalized to 100%, and the runoff rates are normalized accordingly. In general, Figure 13 shows that with the increase of soil water repellency, infiltration is inhibited and runoff is promoted, with less time required to reach the steady state. Three stages can be distinguished for the wettable soil: infiltration, runoff generation and steady state; three stages are also observed for the subcritical water repellent soil: rapid generation of runoff, slow generation of runoff and steady state; two stages are observed for the water repellent soil: runoff generation and steady. The sequence of stages can be used to interpret field data whenever wettability is assumed to be an intervening factor, and could be implemented in models predicting runoff generation in slopes.

The time to ponding is also compared among the different wettability levels in Figure 11a. The

520 time to ponding shows a decrease with an increase in soil water repellency, from 33.1
521 minutes for the wettable soil to 8.8 minutes for the subcritical water repellent soil and 2.5
522 minutes for the water repellent soil, suggesting that the infiltration capacity of the soils is
523 reduced with an increase in soil water repellency. This impact of fire-induced water repellency
524 on the time scale of ponding is consistent with the literature. For example, Zavala et al. (2009)
525 compared the time to ponding values of unaffected soil and fire burned soil, which were ~24
526 minutes and ~4 minutes respectively. Ebel and Moody (2017) collected soil-hydraulic
527 property data from literature review and conducted a meta-analysis to compare unaffected
528 soil and fire-burned soil. The authors reported time to ponding values of tens of minutes for
529 wettable soil and less than one minute for water repellent soil. Although sorptivity is not
530 directly measured in this study, the influence of water repellency on it can be deduced. Since
531 the shortened time to ponding is often attributed to the reduced sorptivity, and consistent
532 changes are observed in this study and literature, it is reasonable to conclude that sorptivity
533 decreases with synthetically induced water repellency. As pointed out by Hallett et al. (2004),
534 sorptivity can be reduced to 50% by water repellency.
535
536 The time to steady state shows a different response with soil water repellency (Figure 11b).
537 The subcritical water repellent soil has the longest time to steady state. From a wettable to a
538 subcritical water repellent condition, the time to steady state increases from 77.5 minutes to
539 88.8 minutes, followed by a decrease to 36.9 minutes for the water repellent soil. A similar
540 trend is observed for the runoff acceleration (Figure 11c) where the subcritical soil achieves
541 the lowest runoff acceleration at 47.9 mm/h^2. The runoff acceleration decreased from 83.3

542 mm/h^2 for the wettable soil to 47.9 mm/h^2 for the subcritical water repellent soil, increasing
543 again to 153.5 mm/h^2 for the water repellent soil.
544
545 Since the time to steady state reflects the duration of the infiltration process, it can be inferred
546 that the longer duration attained by the subcritical water repellent soils is beneficial if they are
547 to be deployed as a fill material, for instance, for man-made or infrastructure slopes. The
548 potential applications of subcritical water repellent soils have been discussed recently (Zheng
549 et al., 2017). Since extreme wettability conditions (wettable and strong water repellency) can
550 cause either landslides or erosion, the optimal conditions that reduce slope instability can be
551 established if subcritical water repellent soil could be deployed on sloping ground. The
552 time-scales for the steady state are longer because of the delayed and prolonged infiltration
553 process. This is further supported by the runoff acceleration, with the subcritical water
554 repellent soil developing the lowest runoff acceleration. These two measurements are not
555 documented in literature and therefore not directly comparable to the results obtained under
556 field conditions, and may be adopted to find the so-called optimal conditions.
557
558 The wetting front rates of all tests are also shown in Figure 11d, indicating a delay in the
559 wetting process with the increase of soil water repellency. Since infiltration was fully
560 prevented by water repellency and no water content change was detected in water repellent
561 soil, its wetting front rate is determined to be 0. The wetting front rate of subcritical water
562 repellent soil (1.0 mm/min) is significantly reduced compared to the wettable soil (2.4
563 mm/min), which is the maximum wetting front rate among the three wettability levels. Fox et

564 al. (2007) studied the effects of fire-induced water repellency on saturated hydraulic
565 conductivity, which decreased by about 37% and 23% for the fine and coarse fractions,
566 respectively. Comparable results were also obtained by Robichaud (2000), when water
567 repellent conditions are present, the saturated hydraulic conductivity of soil reduced between
568 10% and 40% during the onset of simulated rainfall. However, Scott (2000) used an
569 infiltrometer to determine the infiltration rate of water repellent soils, and reported that the
570 results did not prove to be very useful, particularly in that they concentrated at the low end of
571 infiltration rate and could not distinguish between degrees of stronger repellency. This
572 indicates that the hydrological properties of severe or extreme water repellent soil are
573 challenging to obtain through conventional methods.
574
575 The total water storage at the end of each test is presented in Figure 11e. The mean total
576 water storage decreased with an increase in soil water repellency, from 41.9 mm for the
577 wettable soil to 24.2 mm for the subcritical water repellent soil, until 9.3 mm for the water
578 repellent soil.
579
580 Comparable trends albeit involving different processes can be found in the literature. Ebel et
581 al. (2012) and Jordán et al. (2016) monitored the runoff generation immediately after a
582 wildfire and prescribed fire, which revealed some soil water repellency. The post-wildfire ash
583 layer was found to act as a hydrologic buffer to store water at the storm time scale of minutes
584 and then release the water over a period of days. Although the mechanism is different, the
585 roles of the ash layer and the subcritical water repellent soil in controlling runoff are

586 comparable. The results discussed in this section were obtained under field condition and the
587 soil water repellency was incurred by wildfire or prescribed fire, it is possible that the
588 influences of other processes (removal of vegetation cover, surface sealing and pore clogging
589 by ash) are also involved. While in this study, soil water repellency is induced synthetically
590 and its impact is investigated in isolation.
591
592 *4.2. Effects of rainfall intensity, slope angle and relative compaction*
593
594 The RI, slope angle and relative compaction had a limited effect on the hydrological response
595 of the soils as shown by the statistical analysis. However, Ebel and Moody (2017) argued for
596 a need to separate statistical significance from practical hydrologic relevance. Therefore,
597 observed effects or trends between RI, slope angle and relative compaction and the
598 hydrological variables (e.g. time to ponding) is discussed. RI is related to the time to ponding,
599 the time to steady state and the runoff acceleration. High RI leads to less time to ponding and
600 a higher runoff acceleration. A higher wetting front rate (2.9 mm/min) is also linked to a high
601 RI for the wettable soil (2.0 mm/min for low RI), while this effect is not observed for the
602 subcritical water repellent soil. Ebel and Moody (2017) also reported for burned soil more
603 ponding for 100 mm/h rainfall than 20 mm/h rainfall, which is consistent with this study.
604 Dunne et al. (1991) pointed out that for some soils, the infiltration rate is negatively correlated
605 with rainfall intensity because of the development of surface seals, while on soils which do
606 not form seals, the infiltration rate increases with the rainfall intensity. This corresponds to the
607 increased wetting front rate with the increase of rainfall intensity for wettable soil. The relation

608 between water storage and rainfall intensity was investigated by Huang et al. (2013), the
609 water storage after rainfall across the soil profile increased and then decreased as the rainfall
610 intensity grew. This relation was not verified in this study due to the restriction of laboratory
611 test, i.e. only limited amount of water can be stored in the soil.
612
613 The total water storage in the soil is closely related to the slope angle, with steeper slopes
614 leading to a lower total water storage regardless of the wettability level. However, there are
615 substantial disagreements among researchers regarding the impacts of slope angle on
616 infiltration. Fox et al. (1997) reported that infiltration rate decreased with increasing slope
617 angle, and the dominant influence of slope angle on infiltration rate resulted from changes in
618 overland flow depth and surface storage. Chaplot and Le Bissonnais (2000) discovered that
619 infiltration rate reduced with increasing slope gradient for a crusted interrill area. While Ribolzi
620 et al. (2011) conducted field experiments and concluded that infiltration increases with
621 increasing slope steepness, owing to the development of more permeable structural crusts
622 on steeper slopes. Similar view was also shared by Janeau et al. (2003), stating that the
623 steady final infiltration rate increased sharply with increasing slope angle.
624
625 The relative compaction showed little influence on the hydrological response of the soils. For
626 the subcritical repellent and water repellent soils, the wetting front rate was reduced by ~40%
627 and ~100% respectively, comparing to the wettable soil and irrespective of the relative
628 compaction. This implies that the delay in the infiltration process in the subcritical and the
629 water repellent soil remains effective without a close control of the dry density, which may

630 translate into practical benefits when placing these materials in the field. However, relative
631 compaction has been reported to influence hydrological properties of soil. Meek et al. (1992)
632 observed that the infiltration rate and hydraulic conductivity decreased by 53% and 86%
633 respectively, when bulk density was increased from 1.6 to 1.8 Mg/m^3. The contradictory
634 results may result from different initial moisture conditions, in this study the air-dried soil is
635 used whereas the results were obtained under field condition in the literature.
636
637 The combination of the RI, slope angle and relative compaction may also influence the
638 development of the wetting front in the subcritical water repellent soil. The infiltration modes
639 evolved from a parallel wetting front (Figure 9a) to preferential flow (Figure 9b) as the soil
640 wettability changed from wettable to subcritical water repellent. However, due to the different
641 slope angles and relative compactions, two infiltration modes were identified in the subcritical
642 water repellent soil. One refers to preferential flow with horizontal and vertical fingering,
643 showing distinctive wet patches in a dry soil matrix (Figure 9b). The other is an oblique
644 wetting front that saturates from the toe towards the back of the model possibly due to a
645 combination of a high slope angle and high relative compaction (Figure 9c), and together with
646 the accumulation of water in the baffle area (a boundary effect).
647
648 The observed hydrological behavior of synthetic water repellent soils may have implications
649 at the field-scale. For water repellent soils and if they are to be deployed in the stabilization of
650 infrastructure slopes, the field behavior is likely to resemble the model tests where no
651 infiltration is allowed and the response to rainfall is runoff dominated. However, at a

652 catchment scale and in natural water repellent soils, the distribution of natural water repellent
653 soils is known to be patchy implying that the total water storage may increase with the scale.
654 For wettable and subcritical water repellent soils, the time to ponding, time to steady state,
655 runoff acceleration and total water storage are scale-dependent and are likely to increase
656 with the increasing catchment area. The effective rainfall rate does not depend on the scale
657 and the observed hydrological patterns (as in Figure 13) can be expected at larger scales.
658
659 *4.3. DMDCS treatment and capacitance probe*
660
661 The high volumetric water content for the sub-critical water repellent soil may be explained
662 through changes of the electrical conductivity. As observed by Kelleners et al. (2004), the
663 volumetric water content measured by the EC-5 was higher for saline solutions. Thompson et
664 al. (2007) also reported a 4% to 7.5% relative increase in the measured soil water content for
665 every 1 dS/m increase in the electrical conductivity. HCl is a by-product of the reaction
666 between the DMDCS and the OH groups of the soil particles surfaces which requires water
667 for the reaction to complete. After treatment, a small amount of HCl may remain on the soil,
668 resulting in an increased electrical conductivity when water infiltrates. With the continuous
669 subsurface flow, the concentration of HCl reduces with time, with the EC-5 returning to
670 normal at the end of the test (Figure 7b: sensor 1 and 2).
671
672 *4.4. Experimental considerations*
673

674 The raindrop velocity of the artificial rainfall was not measured and is expected to be smaller
675 than the terminal velocity of natural rainfall, owing to the short falling height (~1.5m). This
676 would result in a lower raindrop impact on soil minimizing the effects of rain splash erosion
677 (Vaezi et al., 2017). The terminal velocity of natural raindrops usually ranges from ~2 m/s to
678 ~9 m/s depending on their size (Gunn and Kinzer, 1949), and based on the drop size
679 generated by the nozzle, the terminal velocity of natural raindrops with similar size as in this
680 research is estimated to be around 7 m/s (Wang and Pruppacher, 1977).
681
682 The onset of wetting in all slope models was accurately captured by the moisture sensors.
683 However, the capacitance probes used were influenced by the electrical conductivity,
684 showing unrealistically high volumetric water content for the subcritical water repellent soils.
685 Due to this, only the timing of the moisture change was used in the analysis. In the future,
686 other types of dielectric sensors such as TDR should be used to obtain the volumetric water
687 content, to avoid the influence of electrical conductivity when working with treated soil. In
688 addition, the EC-5 is known for being sensitive to changes in bulk density, with the output
689 increasing with the bulk density (Parsons and Bandaranayake, 2009).
690
691 The lower boundary of the slope model influenced the hydrological response of the soil.
692 There was excessive infiltration near the baffle area due to the accumulation of water from
693 the subsurface flow and due to the wettable nature of the baffle (acting as a preferential
694 infiltration interface) (Figure 9). This response was included in the data analysis leading to an
695 overestimation of the effective rainfall rate and total water storage. The thickness of the soil

696 was only 10 cm and water was unable to drain out of the bottom of the flume. Then the
697 subsurface flow had to drain out of the baffle, the runoff measured included both surface and
698 subsurface runoff, and cannot be distinguished. This limitation in experimental setting needs
699 to be considered in the future. Direct measurement of soil-hydraulic properties (e.g. saturated
700 hydraulic conductivity, sorptivity etc.) should also be considered to allow comparison with
701 other field and laboratory investigations.
702
703 **Conclusion**
704
705 Analysis of experimental data from a series of 24 flume tests in completely decomposed
706 granite from Hong Kong at various soil water repellency levels, rainfall intensities, slope
707 angles and relative compactions revealed that: (1) An increase in water repellency leads to a
708 significant drop in both the wetting front rate (by ~40% and ~100% for the subcritical water
709 repellent and water repellent soil, respectively) and the total water storage (by ~42% and ~77%
710 for the subcritical water repellent and water repellent soil, respectively), (2) The time to
711 ponding is shortened by an increase in water repellency (by ~74% and ~92% for the
712 subcritical water repellent and water repellent soil, respectively), (3) The time to steady state
713 is longest for the subcritical water repellent soils implying that the infiltration process is longer
714 in duration than for the wettable and water repellent soils, (4) Different runoff hydrographs
715 were identified with infiltration modes ranging from a parallel wetting front (wettable soils) to
716 preferential flow and an oblique wetting front (for the subcritical water repellent soils,
717 depending on the slope angle and relative compaction).

718

719 The effect of rainfall intensity on the slope hydrology contrasted with that of the relative
720 compaction. The increased rainfall intensity leads to shorter times to ponding and to steady
721 state, as well as a higher runoff acceleration but none of these parameters were sensitive to
722 the relative compaction. This implies that the delaying effect of water repellency on infiltration
723 remains effective without requiring precise control of the relative compaction. For the slope
724 angle, the total water storage was the only sensitive parameter increasing with a decrease of
725 the slope angle.

726

727 While the trends obtained and processes identified in this study can be extended to
728 man-made slopes and natural catchments with water repellent soils, the tested conditions
729 were not extreme and were not able to capture all the processes that lead to extreme field
730 events such as post-wildfire debris flows. For instance, the rather finer nature of the soils and
731 a maximum rainfall intensity only at 70 mm/h, inhibited the development of overland flow and
732 erosion. Future work will define the threshold conditions for these processes to initiate.
733 However, the current research highlights the interplay between soil wettability and rainfall
734 intensity in slope hydrology and promotes our understanding of natural runoff generation
735 when soil wettability is considered in isolation.

736

737 **Acknowledgements**

738

739 This research was supported by the Research Grants Council of Hong Kong, grants

17205915 and T22-603/15-N. The testing material was provided by the Drainage Services Department, Hong Kong Government. Laboratory assistance by Mr. N. C. Poon and Mr. Xu Dong is acknowledged. We thank the three anonymous reviewers whose comments helped improve and clarify this manuscript.

745 **References**

746

747 Ahn, S., Doerr, S. H., Douglas, P., Bryant, R., Hamlett, C. A. E., McHale, G., Newton, M. I.,
748 Shirtcliffe, N. J. (2013). Effects of hydrophobicity on splash erosion of model soil particles
749 by a single water drop impact. Earth Surface Processes and Landforms, 38(11),
750 1225-1233.

751 Bachmann, J., Ellies, A., & Hartge, K. (2000). Development and application of a new sessile
752 drop CA method to assess soil water repellency. Journal of Hydrology, 231, 66-75.

753 Bardet, J.-P., Jesmani, M., & Jabbari, N. (2014). Permeability and compressibility of
754 wax-coated sands. Géotechnique, 64(5), 341-350.

755 Bisdom, E., Dekker, L., & Schoute, J. T. (1993). Water repellency of sieve fractions from
756 sandy soils and relationships with organic material and soil structure. Geoderma, 56(1-4),
757 105-118.

758 BS 1377-3:1990, 1990. Methods of test for soils for civil engineering purposes. Chemical and
759 electro-chemical tests. BSI, UK.

760 Cannon, S. H., Gartner, J. E., Wilson, R. C., Bowers, J. C., & Laber, J. L. (2008). Storm
761 rainfall conditions for floods and debris flows from recently burned areas in southwestern
762 Colorado and southern California. Geomorphology, 96(3-4), 250-269.

763 Chaplot, V., & Le Bissonnais, Y. (2000). Field measurements of interrill erosion under different
764 slopes and plot sizes. Earth Surface Processes and Landforms, 25(2), 145-153.

765 Choi, Y., Choo, H., Yun, T., Lee, C., & Lee, W. (2016). Engineering Characteristics of
766 Chemically Treated Water-Repellent Kaolin. Materials, 9(12), 978.

767 Cobos, D. R., & Chambers, C. (2010). Calibrating ECH2O soil moisture sensors. Application
768 Note, Decagon Devices, Pullman, WA.
769 Czachor, H., Doerr, S., & Lichner, L. (2010). Water retention of repellent and subcritical
770 repellent soils: New insights from model and experimental investigations. Journal of
771 Hydrology, 380(1), 104-111.
772 DeBano, L. F. (1981). Water repellent soils: a state-of-the-art. USDA Forest Service General
773 Technical Report PS W-46 (22p).
774 DeBano, L. (2000). Water repellency in soils: a historical overview. Journal of Hydrology, 231,
775 4-32.
776 Dell'Avanzi, E., Guizelini, A., da Silva, W., & Nocko, L. (2010). Potential use of induced
777 soil-water repellency techniques to improve the performance of landfill's alternative final
778 cover systems. Unsaturated soils. CRC Press, Boca Raton, FL, 461-466.
779 Diskin, M. H., & Nazimov, N. (1996). Ponding time and infiltration capacity variation during
780 steady rainfall. Journal of Hydrology, 178(1–4), 369-380.
781 Doerr, S. H. (1998). On standardizing the 'water drop penetration time' and the 'molarity of an
782 ethanol droplet' techniques to classify soil hydrophobicity: a case study using medium
783 textured soils. Earth Surface Processes and Landforms, 23(7), 663-668.
784 Doerr, S. H., Shakesby, R. A., Blake, W. H., Chafer, C. J., Humphreys, G. S., & Wallbrink, P. J.
785 (2006). Effects of differing wildfire severities on soil wettability and implications for
786 hydrological response. Journal of Hydrology, 319(1-4), 295-311.
787 Drainage Services Department. (2013). Stormwater drainage manual: Planning, Design and
788 Management, 4th Edition. Government of the Hong Kong Special Administrative Region,

789 Hong Kong.
790 Dunne, T., Zhang, W., & Aubry, B. F. (1991). Effects of Rainfall, Vegetation, and
791 Microtopography on Infiltration and Runoff. Water Resources Research, 27(9),
792 2271-2285.
793 Ebel, B. A., Moody, J. A., & Martin, D. A. (2012). Hydrologic conditions controlling runoff
794 generation immediately after wildfire. Water Resources Research, 48(3). W03529.
795 Ebel, B. A., & Moody, J. A. (2017). Synthesis of soil-hydraulic properties and infiltration
796 timescales in wildfire-affected soils. Hydrological Processes, 31(2), 324-340.
797 Eckersley, D. (1990). Instrumented laboratory flowslides. Géotechnique, 40(3), 489-502.
798 Fox, D. M., Bryan, R. B., & Price, A. G. (1997). The influence of slope angle on final infiltration
799 rate for interrill conditions. Geoderma, 80(1), 181-194.
800 Fox, D. M., Darboux, F., & Carrega, P. (2007). Effects of wildfire-induced water repellency on
801 soil aggregate stability, splash erosion, and saturated hydraulic conductivity for different
802 size fractions. Hydrological Processes, 21(17), 2377-2384.
803 Gunn, R., & Kinzer, G. D. (1949). The teminal volocity of fall for water droplets in stagnant air.
804 Journal of Meteorology, 6(4), 243-248.
805 Hallett, P. D., Nunan, N., Douglas, J. T., & Young, I. M. (2004). Millimeter-scale spatial
806 variability in soil water sorptivity. Soil Science Society of America Journal, 68, 352–358.
807 Hamlett, C. A. E., Atherton, S., Shirtcliffe, N. J., McHale, G., Ahn, S., Doerr, S. H., Bryant, R.,
808 Newton, M. I. (2013). Transitions of water-drop impact behaviour on hydrophobic and
809 hydrophilic particles. European Journal of Soil Science, 64(3), 324-333.
810 Huang, J., Wu, P., & Zhao, X. (2013). Effects of rainfall intensity, underlying surface and slope

811 gradient on soil infiltration under simulated rainfall experiments. Catena, 104, 93-102.
812 Iverson, R. M., & LaHusen, R. G. (1993). Friction in debris flows: inferences from
813 large-scale flume experiments. In American Society of Civil Engineers, Hydraulic
814 Engineering ’93 Conference, San Francisco, California, July 25–30 1993, Proceedings, p.
815 1604–1609.
816 Janeau, J.L., Briquet, J.P., Planchon, O., Valentin, C. (2003). Soil crusting and infiltration on
817 steep slopes in northern Thailand. European Journal of Soil Science, 54(3), 543–553.
818 Jordán, A., Zavala, L. M., Granged, A. J. P., Gordillo-Rivero, Á. J., García-Moreno, J., Pereira,
819 P., . . . Alanís, N. (2016). Wettability of ash conditions splash erosion and runoff rates in
820 the post-fire. Science of The Total Environment, 572, 1261-1268.
821 Kean, J. W., Staley, D. M., Leeper, R. J., Schmidt, K. M., & Gartner, J. E. (2012). A low-cost
822 method to measure the timing of postwildfire flash floods and debris flows relative to
823 rainfall. Water Resources Research, 48(5), W05516.
824 Kelleners, T. J., Soppe, R. W. O., Ayars, J. E., & Skaggs, T. H. (2004). Calibration of
825 Capacitance Probe Sensors in a Saline Silty Clay Soil. Soil Science Society of America
826 Journal, 68(3), 770-778.
827 Kruskal, W. H., & Wallis, W. A. (1952). Use of ranks in one-criterion variance analysis. Journal
828 of the American Statistical Association, 47, 583–621.
829 Lee, C., Yang, H.-J., Yun, T. S., Choi, Y., & Yang, S. (2015). Water-Entry Pressure and
830 Friction Angle in an Artificially Synthesized Water-Repellent Silty Soil. Vadose Zone
831 Journal, 14(4).
832 Leelamanie, D., & Karube, J. (2009). Time dependence of CA and its relation to repellency

persistence in hydrophobized sand. Soil Science and Plant Nutrition, 55(4), 457-461.

Li, P. W., & Lai, E. S. T. (2004). Short-range quantitative precipitation forecasting in Hong Kong. Journal of Hydrology, 288(1-2), 189-209.

Lourenço, S. D. N., Sassa, K., & Fukuoka, H. (2006). Failure process and hydrologic response of a two layer physical model: Implications for rainfall-induced landslides. Geomorphology, 73(1), 115-130.

Lourenço, S. D. N., Jones, N., Morley, C., Doerr, S. H., & Bryant, R. (2015a). Hysteresis in the Soil Water Retention of a Sand-Clay Mixture with CAs Lower than Ninety Degrees. Vadose Zone Journal, 14(7).

Lourenço, S., Woche, S., Bachmann, J., & Saulick, Y. (2015b). Wettability of crushed air-dried minerals. *Géotechnique Letters, 5*(3), 173-177.

Lourenço, S. D. N., Wang, G.-H., & Kamai, T. (2015c). Processes in model slopes made of mixtures of wettable and water repellent sand: Implications for the initiation of debris flows in dry slopes. Engineering Geology, 196, 47-58.

Lumb, P. (1965). The residual soils of Hong Kong. Géotechnique, 15(2), 180-194.

Meek, B. D., Rechel, E., Carter, L. M., DeTar, W. R., & Urie, A. (1992). Infiltration rate of a sandy loam soil: effects of traffic, tillage, and plant roots. Soil Science Society of America Journal, 56(3), 908-913.

Meyers, L., & Frasier, G. W. (1969). Creating hydrophobic soil for water harvesting. Journal of Irrigation and Drainage Engineering, 95, 43-54.

Ng, S. H. Y., & Lourenço, S. D. N. (2016). Conditions to induce water repellency in soils with dimethyldichlorosilane. Géotechnique, 66(5), 441-444.

855 Parsons, L. R., & Bandaranayake, W. M. (2009). Performance of a new capacitance soil
856 moisture probe in a sandy soil. Soil Science Society of America Journal, 73(4),
857 1378-1385.
858 Ribolzi, O., Patin, J., Bresson, L. M., Latsachack, K. O., Mouche, E., Sengtaheuanghoung,
859 O., . . . Valentin, C. (2011). Impact of slope gradient on soil surface features and
860 infiltration on steep slopes in northern Laos. Geomorphology, 127(1), 53-63.
861 Ritsema, C. J., & Dekker, L. W. (2000). Preferential flow in water repellent sandy soils:
862 principles and modeling implications. Journal of Hydrology, 231-232, 308-319.
863 Robichaud, P. R. (2000). Fire effects on infiltration rates after prescribed fire in Northern
864 Rocky Mountain forests, USA. Journal of Hydrology, 231, 220-229.
865 Robichaud, P. R., Wagenbrenner, J. W., Pierson, F. B., Spaeth, K. E., Ashmun, L. E., & Moffet,
866 C. A. (2016). Infiltration and interrill erosion rates after a wildfire in western Montana,
867 USA. Catena, 142, 77-88.
868 Saulick, Y., Lourenço, S. D. N., & Baudet, B. A. (2017). A Semi-Automated Technique for
869 Repeatable and Reproducible Contact Angle Measurements in Granular Materials using
870 the Sessile Drop Method. Soil Science Society of America Journal, 81(2), 241-249.
871 Scott, D. F. (2000). Soil wettability in forested catchments in South Africa; as measured by
872 different methods and as affected by vegetation cover and soil characteristics. Journal of
873 Hydrology, 231, 87-104.
874 Stoof, C. R., Slingerland, E. C., Mol, W., Van Den Berg, J., Vermeulen, P. J., Ferreira, A. J.
875 D., . . . Steenhuis, T. S. (2014). Preferential flow as a potential mechanism for
876 fire-induced increase in streamflow. Water Resources Research, 50(2), 1840-1845.

877 Sun, H. W. (1999). Review of fill slope failures in Hong Kong. GEO Report No. 96.
878 Geotechnical Engineering Office, Civil Engineering Department, 87 pp.
879 Thompson, R. B., Gallardo, M., Fernández, M. D., Valdez, L. C., & Martínez-Gaitán, C. (2007).
880 Salinity Effects on Soil Moisture Measurement Made with a Capacitance Sensor. Soil
881 Science Society of America Journal, 71(6), 1647-1657.
882 Tohari, A., Nishigaki, M., & Komatsu, M. (2007). Laboratory rainfall-induced slope failure with
883 moisture content measurement. Journal of Geotechnical and Geoenvironmental
884 Engineering, 133(5), 575-587.
885 Vaezi, A. R., Ahmadi, M., & Cerdà, A. (2017). Contribution of raindrop impact to the change of
886 soil physical properties and water erosion under semi-arid rainfalls. Science of The Total
887 Environment, 583, 382-392.
888 Wang, G., & Sassa, K. (2001). Factors affecting rainfallinduced flowslides in laboratory flume
889 tests. Géotechnique, 51(7), 587-599.
890 Wang, P. K., & Pruppacher, H. R. (1977). Acceleration to Terminal Velocity of Cloud and
891 Raindrops. Journal of Applied Meteorology, 16(3), 275-280.
892 Wijewardana, N. S., Kawamoto, K., Moldrup, P., Komatsu, T., Kurukulasuriya, L. C., &
893 Priyankara, N. H. (2015). Characterization of water repellency for hydrophobized grains
894 with different geometries and sizes. Environmental Earth Sciences, 74(7), 5525-5539.
895 Zavala, L. M., Jordán, A., Gil, J., Bellinfante, N., & Pain, C. (2009). Intact ash and charred
896 litter reduces susceptibility to rain splash erosion post-wildfire. Earth Surface Processes
897 and Landforms, 34, 1522–1532.
898 Zhang, H. Y., Zhu, S. B., Li, M., & Zhang, X. C. (2016). Water Repellency of Monument Soil

899 Treated by Tung Oil. Geotechnical and Geological Engineering, 34(1), 205-216.

900 Zheng, S., Lourenço, S. D. N., Cleall, P. J., Millis, S. W., Ng, A. K. Y., & Chui, T. F. M. (2017).

901 Synthetic Water Repellent Soils for Slope Stabilization. In M. Mikoš, Ž. Arbanas, Y. Yin, &

902 K. Sassa (Eds.), *Advancing Culture of Living with Landslides: Volume 3 Advances in*

903 *Landslide Technology* (pp. 523-528). Cham: Springer International Publishing.

904

905 **Captions of figures and tables**

906

907 Table 1: Physical properties of Completely Decomposed Granite.

908 Table 2: Levels of water repellency and corresponding water drop penetration time. *After*

909 Doerr (1998).

910 Table 3: Summary of flume tests.

911 Table 4: Statistical analysis on impacts of rainfall intensity, slope angle, relative compaction

912 and initial wettability (significance level = 0.05).

913

914 Figure 1: Particle size distribution of CDG.

915 Figure 2. WDPT and CAs for CDG as percentage by soil mass of DMDCS.

916 Figure 3. CAs of CDG with time after treatment.

917 Figure 4. Configuration of flume model. (a) Schematic illustration of dimensions and

918 instruments. (b) View of the flume installation.

919 Figure 5: Schematic for the variables used; runoff rate (q); effective rainfall rate (i); time to

920 ponding (t_p); time to steady state (t_{ss}); runoff acceleration (a_q); total water storage (S).

921 Figure 6. Time series data for a flume test with wettable soil (test 1). (a) Runoff rate and

922 effective rainfall rate. (b) Volumetric water content at various locations.

923 Figure 7. Time series data for a flume test with subcritical water repellent soil (test 8). (a)

924 Runoff rate and effective rainfall rate. (b) Volumetric water content at various locations.

925 Figure 8. Time series data for a flume test with water repellent soil (test 15). (a) Runoff rate

926 and effective rainfall rate. (b) Volumetric water content at various locations.

927 Figure 9. Photographs of the infiltration modes, black and white color denote wet and dry
928 zones respectively, dotted red line indicates extent of wetting front (slope toes are at the
929 left-hand side of photos, upper 9 cm of the slope shown). (a) Wettable soil (test 1). (b)
930 Subcritical water repellent soil (test 11). (c) Subcritical water repellent soil (test 8). (d) Water
931 repellent soil (test 3).
932 Figure 10. Calibration equations of EC-5 with wettable and subcritical water repellent soils.
933 Figure 11. Effects of rainfall intensity and slope angle on different soils. (a) Effect of rainfall
934 intensity (RI) on time to ponding. (b) Effect of rainfall intensity (RI) on time to steady state. (c)
935 Effect of rainfall intensity (RI) on runoff acceleration. (d) Effect of rainfall intensity (RI) on
936 wetting front rate. (e) Effect of slope angle (SA) on total water storage.
937 Figure 12. Cross section near the slope toe after test: evidence of leak between the baffle and
938 slope (test 3).
939 Figure 13. Runoff hydrographs of soils with various wettability (tests 8, 13, 15).

Tables and Figures

Table 1: Physical properties of Completely Decomposed Granite.

Parameters (unit)	**Values**
Specific gravity, G_s	2.65
Optimum water content	23%
Maximum dry density (g/cm^3)	1.57
Coefficient of uniformity, Cu	690
Coefficient of curvature, Cc	2.32
Maximum void ratio, e_{max}	1.37
Organic matter content	1.95%

Table 2: Levels of water repellency and corresponding water drop penetration time. *After* Doerr (1998).

Water repellency level	**WDPT (s)**
Wettable	⩽5 s
Slightly water repellent	5-60 s
Strongly water repellent	60-600 s
Severely water repellent	600-3600 s
Extremely water repellent	⩾3600 s

Table 3: Summary of flume test.

Test No.	Test settings					Test results				
	Initial volumetric water content (%)	**CA (°)**	**Relative compaction (%)**	**Slope angle(°)**	**Rainfall intensity (mm/h)**	**Time to ponding (t_p, min)**	**Time to steady state (t_{ss}, min)**	**Runoff acceleration (a_q, mm/h^2)**	**Total water storage (S, mm)**	**Wetting front rate (v_{wf}, mm/min)**
1	9.16	55	90	20	74.4±4.6	20	55	164.06	49.24	3.13
2	16.8	90				0	70	83.83	23.61	0.57
3	13.2	120				0	50	107.42	25.52	0.00
4	0.9	55	70			20	70	94.19	46.43	2.78
5	4.1	90				10	110	46.31	41.16	1.52
6	1.0	120				5	20	332.40	13.18	0.00
7	7.6	55	90	40	69.8±6.1	25	85	72.41	47.06	1.89
8	11.1	90				0	95	55.63	30.84	0.69
9	11.6	120				0	45	99.40	6.80	0.00
10	1.9	55	70			20	50	176.03	38.62	3.70
11	1.9	90				0	40	84.43	11.31	0.48

12	12.3	120				0	45	134.10	9.32	0.00
13	5.1	55	90	20	34.2±3.3	50	75	118.62	42.26	3.23
14	14.0	90				15	85	42.88	36.81	1.43
15	7.6	120				0	30	98.25	6.36	0.00
16	1.0	55	70			30	100	41.72	43.74	1.79
17	3.2	90				15	110	29.34	24.86	1.37
18	10.7	120				5	15	342.00	6.46	0.00
19	8.2	55	90	40	30.4±1.8	60	90	64.35	34.41	1.27
20	7.1	90				15	105	20.55	14.35	0.68
21	6.6	120				5	30	80.91	4.32	0.00
22	0.8	55	70			40	95	33.87	33.30	1.72
23	1.2	90				15	95	20.00	10.98	-
24	11.9	120				5	60	33.87	5.24	0.00

Table 4: Statistical analysis on impacts of rainfall intensity, slope angle, relative compaction and initial wettability (significance level = 0.05).

		Time to ponding		Time to steady state		Runoff acceleration		Wetting front rate		Total water storage	
Rainfall intensity	Values	30 mm/h	70 mm/h	30 mm/h	70 mm/h	30 mm/h	70 mm/h	30 mm/h	70 mm/h	30 mm/h	70 mm/h
	n=	12	12	12	12	12	12	12	12	12	12
	Mean	21.25	38.3	74.17	61.25	77.20	120.85	1.64	1.84	21.92	28.59
	Standard deviation	19.44	10.08	32.67	25.60	89.15	77.49	0.79	1.25	15.53	15.86
	p-value	0.0731		0.2927		0.0179		0.4775		0.3094	
Slope angle	Values	20°	40°	20°	40°	20°	40°	20°	40°	20°	40°
	n=	12	12	12	12	12	12	12	12	12	12
	Mean	14.17	15.42	65.83	69.58	125.08	72.96	1.32	0.87	29.97	20.55
	Standard deviation	14.75	18.76	32.88	26.92	106.33	46.94	1.24	1.13	15.47	15.13
	p-value	0.8577		0.7627		0.1841		0.3638		0.1489	
Relative compaction	Values	70%	90%	70%	90%	70%	90%	70%	90%	70%	90%
	n=	12	12	12	12	12	12	12	12	12	12

	Mean	13.75		15.83	67.50		67.92	114.02		84.03	1.11		1.07	23.72		26.80
	Standard deviation	12.27		20.43	34.15		25.45	114.36		37.72	1.25		1.16	15.98		16.00
	p-value	0.7649			0.9733			0.7728			0.9355			0.6861		
Contact angle	Values	55°	90°	120°	55°	90°	120°	55°	90°	120°	55°	90°	120°	55°	90°	120°
	n=	8	8	8	8	8	8	8	8	8	8	8	8	8	8	8
	Mean	33.13	8.75	2.50	77.50	88.75	36.88	95.66	47.87	153.54	2.44	0.84	0.00	41.88	24.24	9.65
	Standard deviation	15.34	7.44	2.67	18.32	23.87	15.57	53.34	25.59	116.86	0.88	0.54	0.00	5.92	11.52	6.98
	p-value	0.0002			7.126e-05			0.0204			0.0014			9.427e-07		

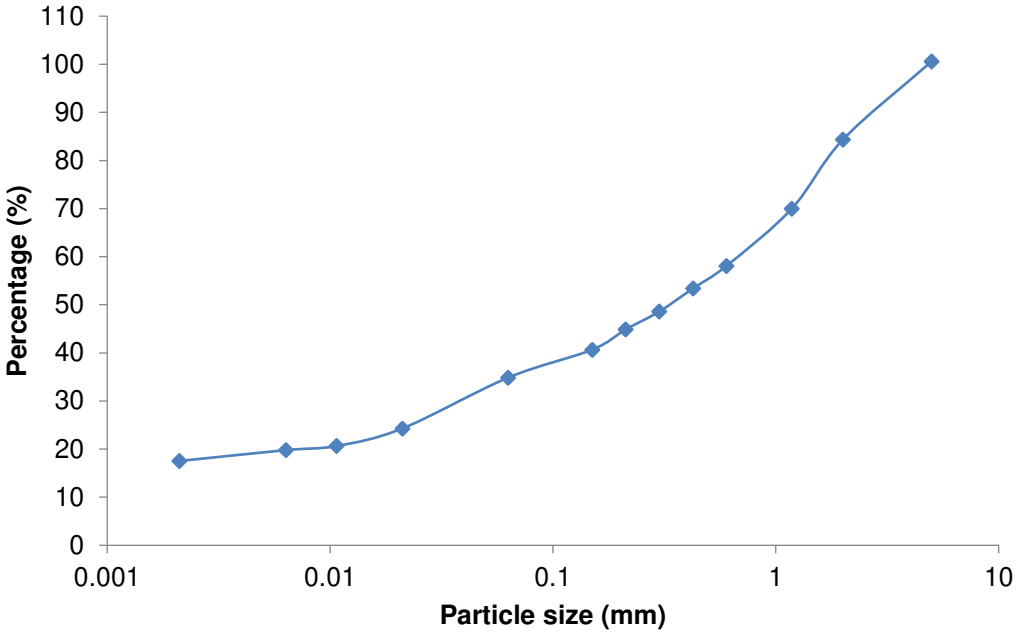

Figure 1: Particle size distribution of CDG.

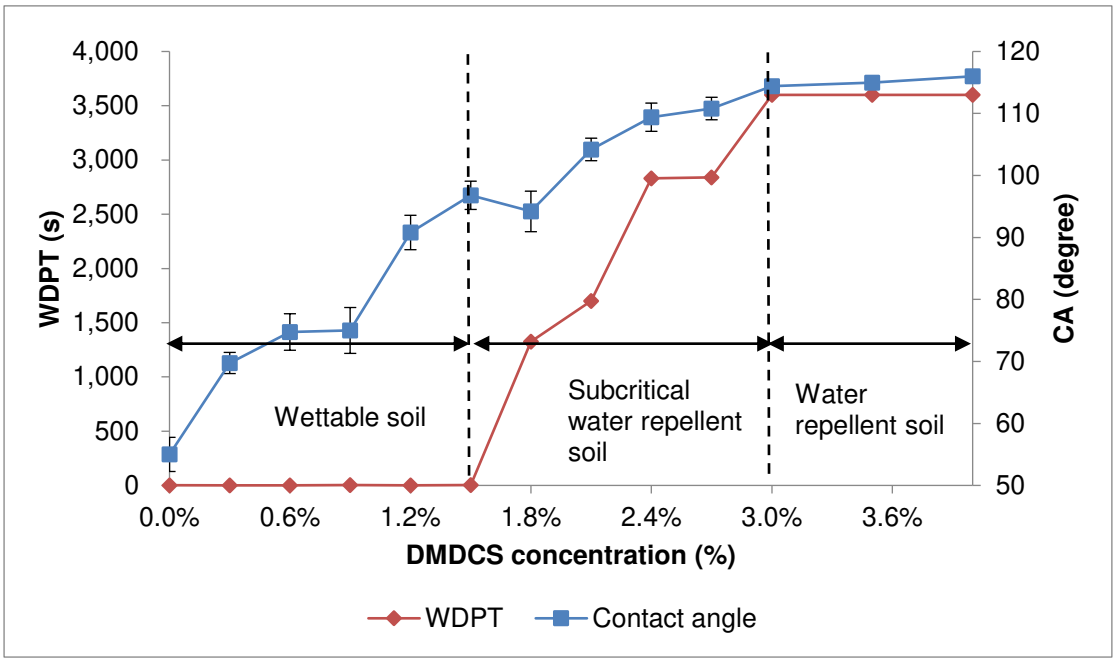

Figure 2. WDPT and CAs for CDG as percentage by soil mass of DMDCS.

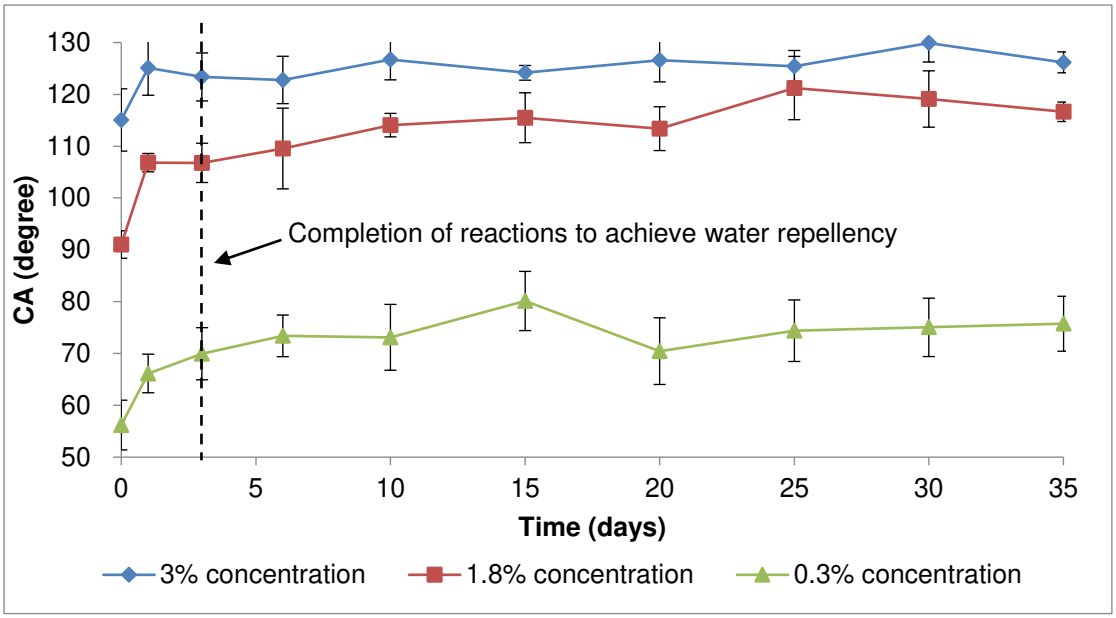

Figure 3. CAs of CDG with time after treatment.

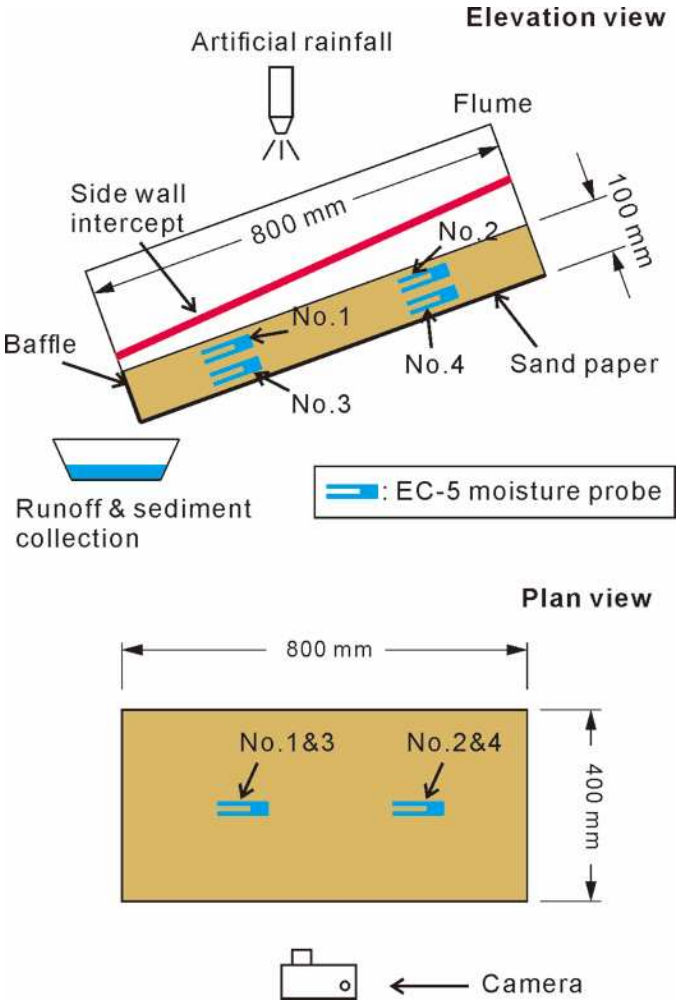

a

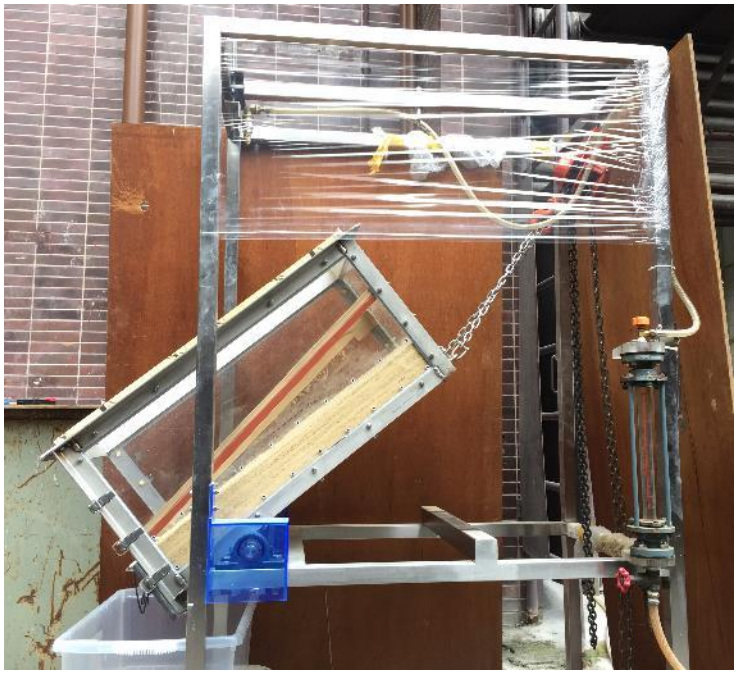

b

Figure 4. Configuration of flume model. (a) Schematic illustration of dimensions and instruments. (b) View of the flume installation.

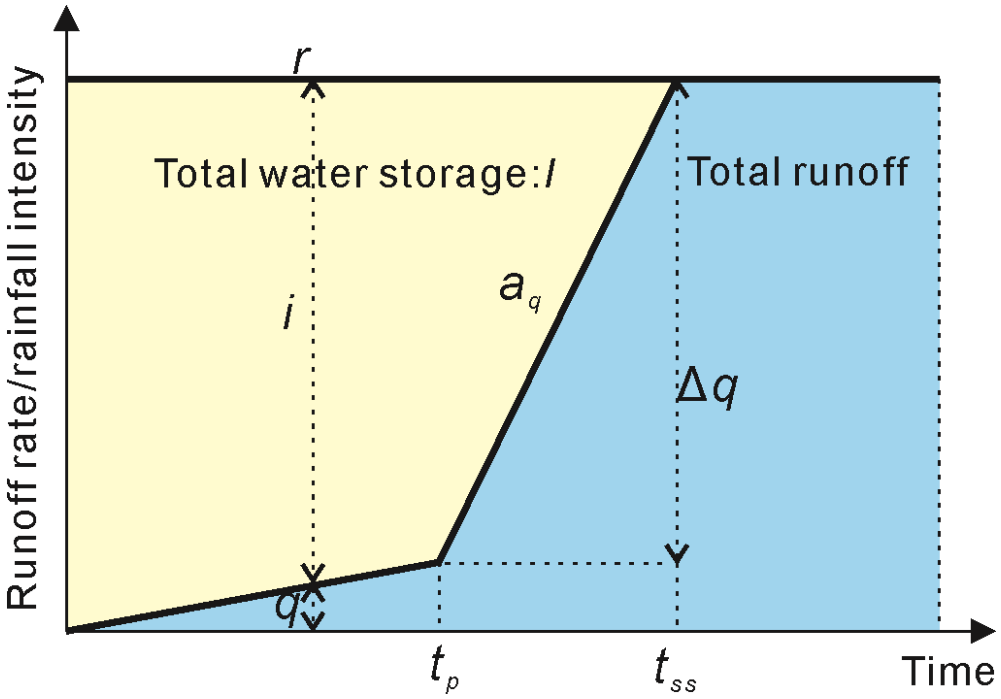

Figure 5: Schematic for the variables used; runoff rate (q); effective rainfall rate (i); time to ponding (t_p); time to steady state (t_{ss}); runoff acceleration (a_q); total water storage (S).

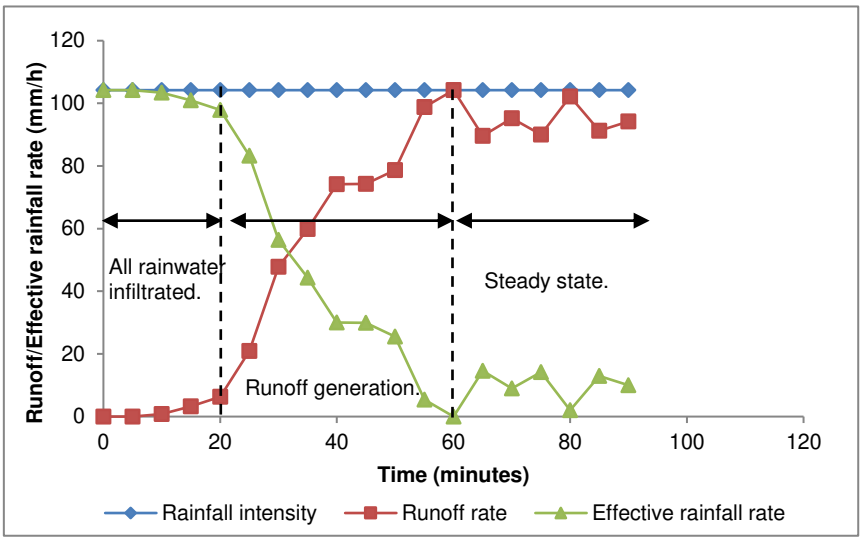

a

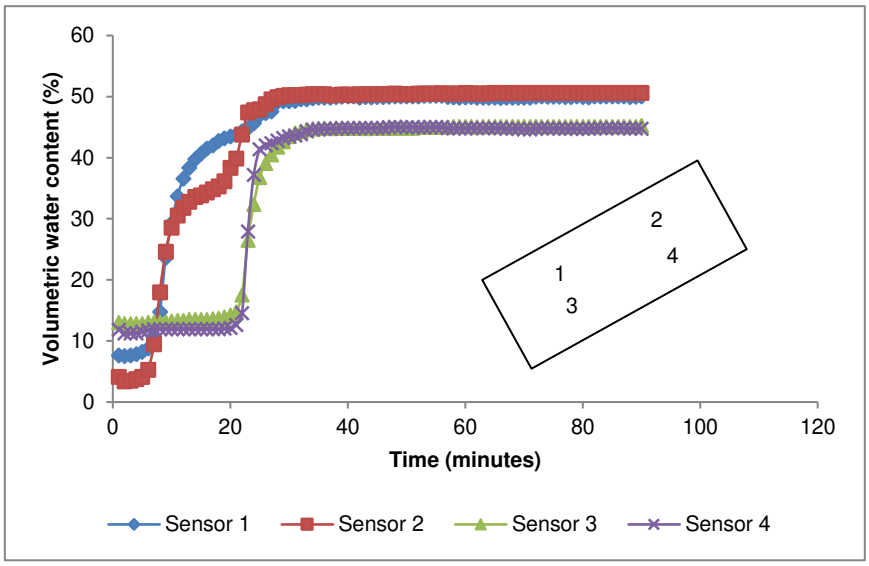

b

Figure 6. Time series data for a flume test with wettable soil (test 1). (a) Runoff rate and effective rainfall rate. (b) Volumetric water content at various locations.

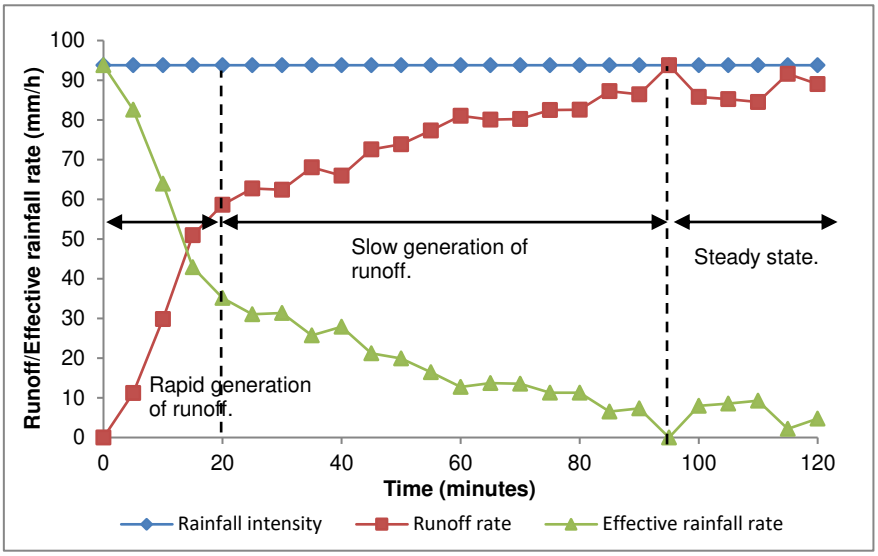

a

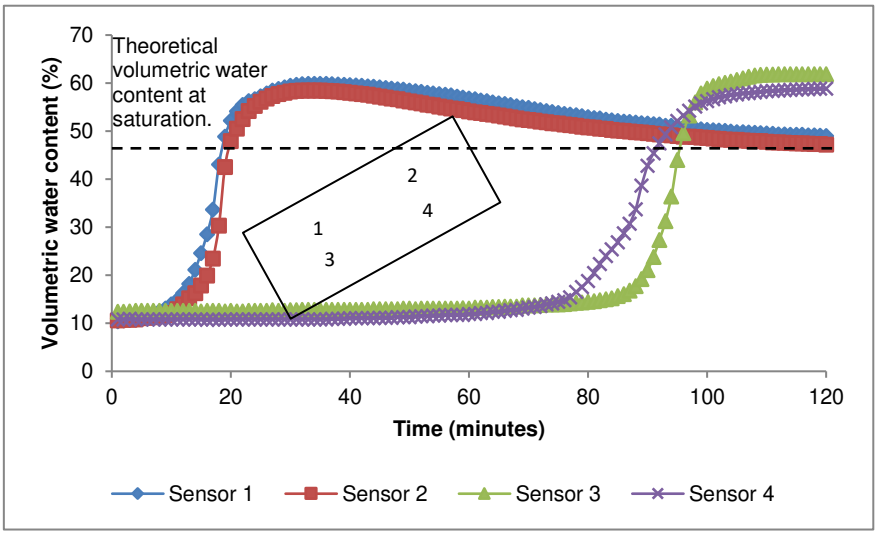

b

Figure 7. Time series data for a flume test with subcritical water repellent soil (test 8). (a) Runoff rate and effective rainfall rate. (b) Volumetric water content at various locations.

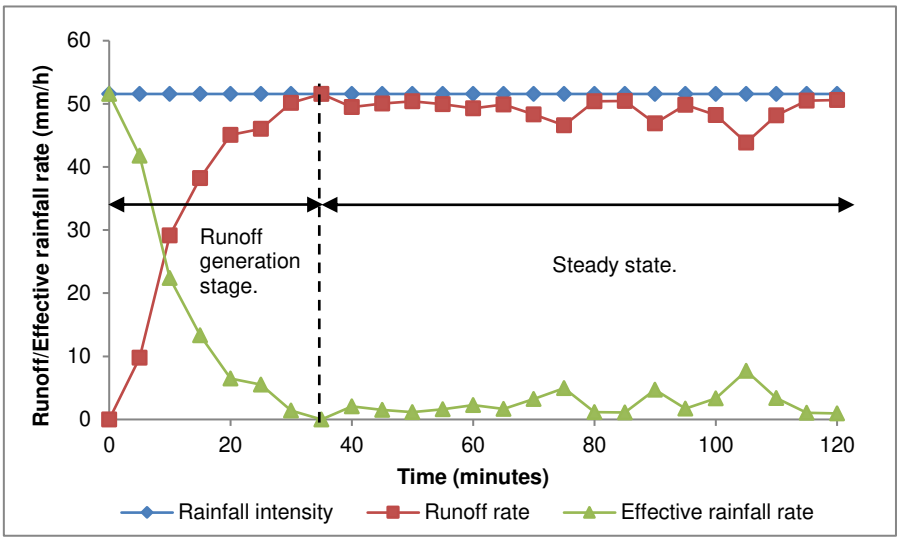

a

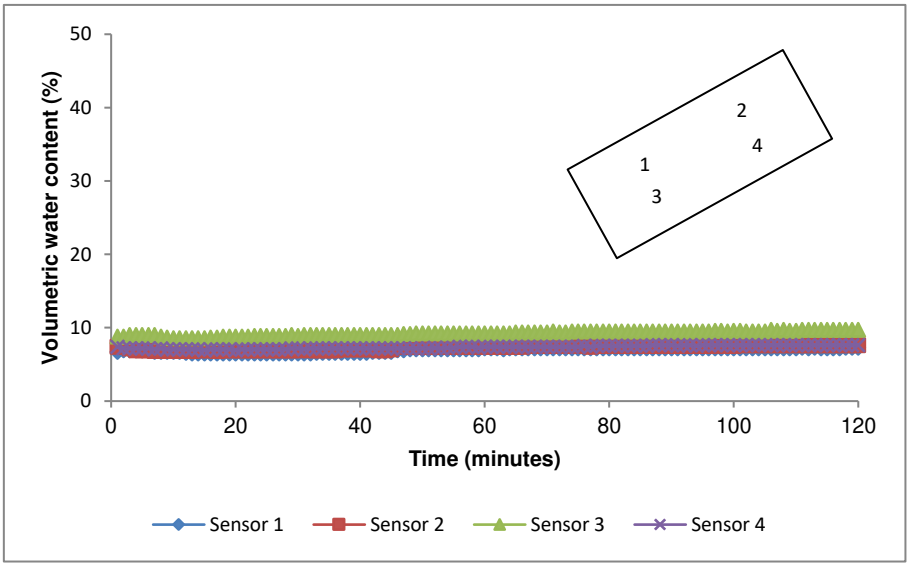

b

Figure 8. Time series data for a flume test with water repellent soil (test 15). (a) Runoff rate and effective rainfall rate. (b) Volumetric water content at various locations.

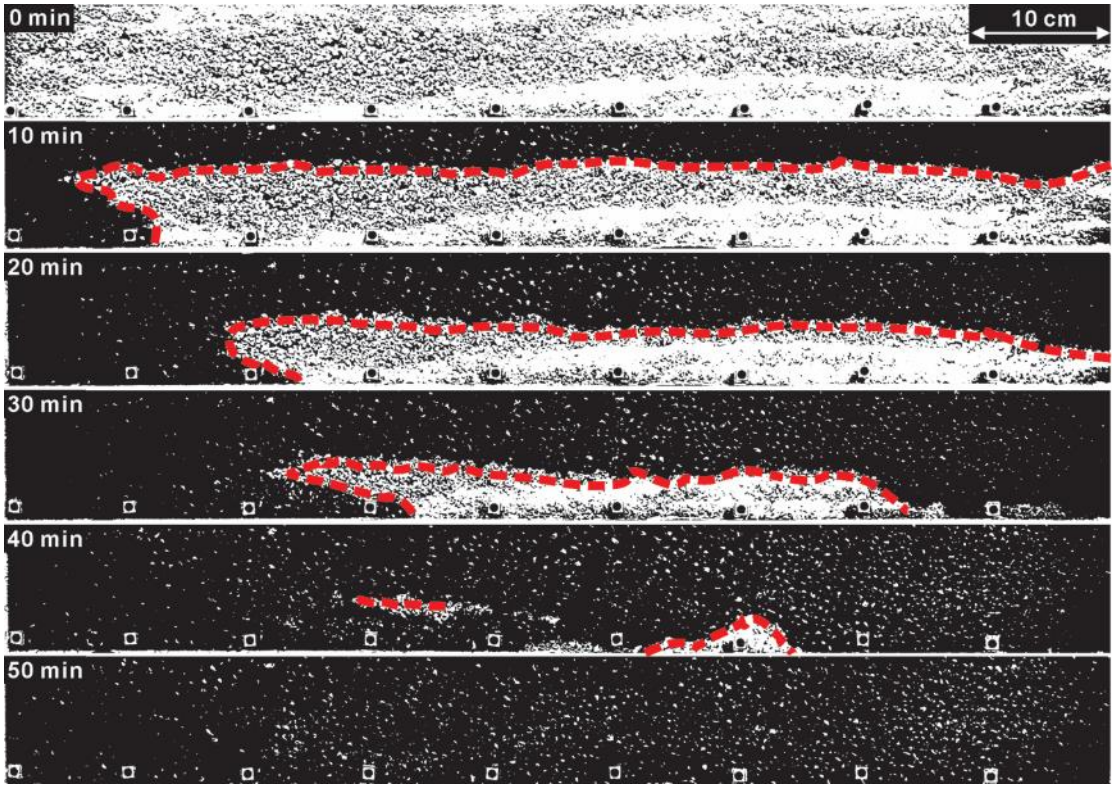
0 min
10 cm
10 min
20 min
30 min
40 min
50 min

a

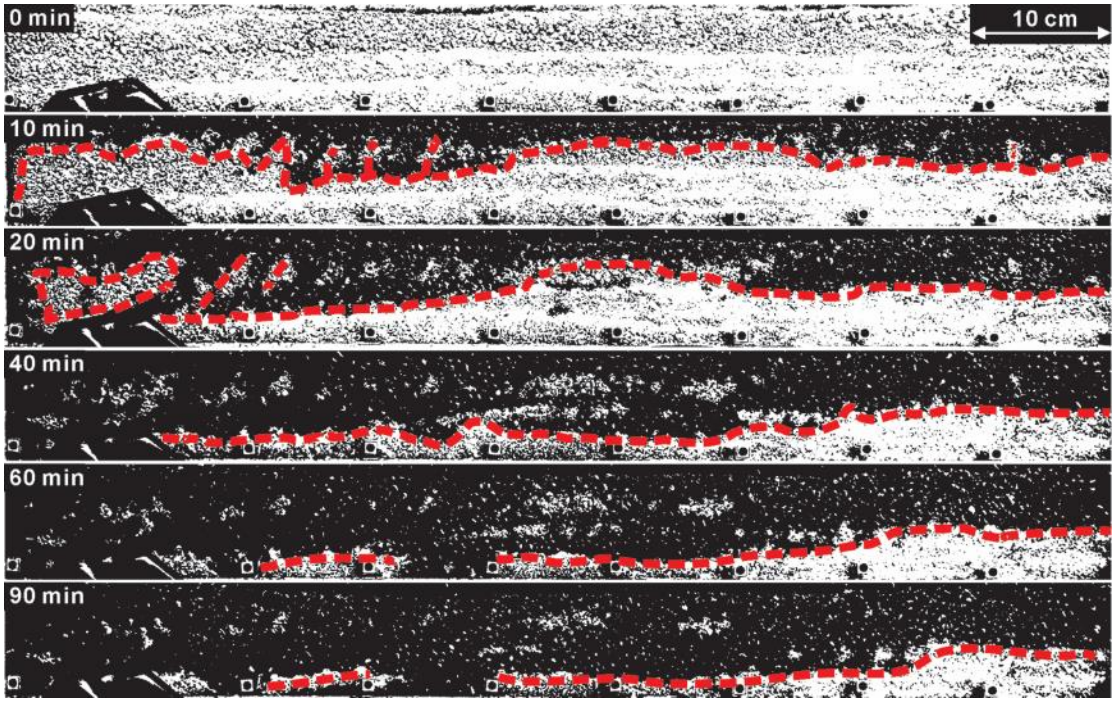
0 min
10 cm
10 min
20 min
40 min
60 min
90 min

b

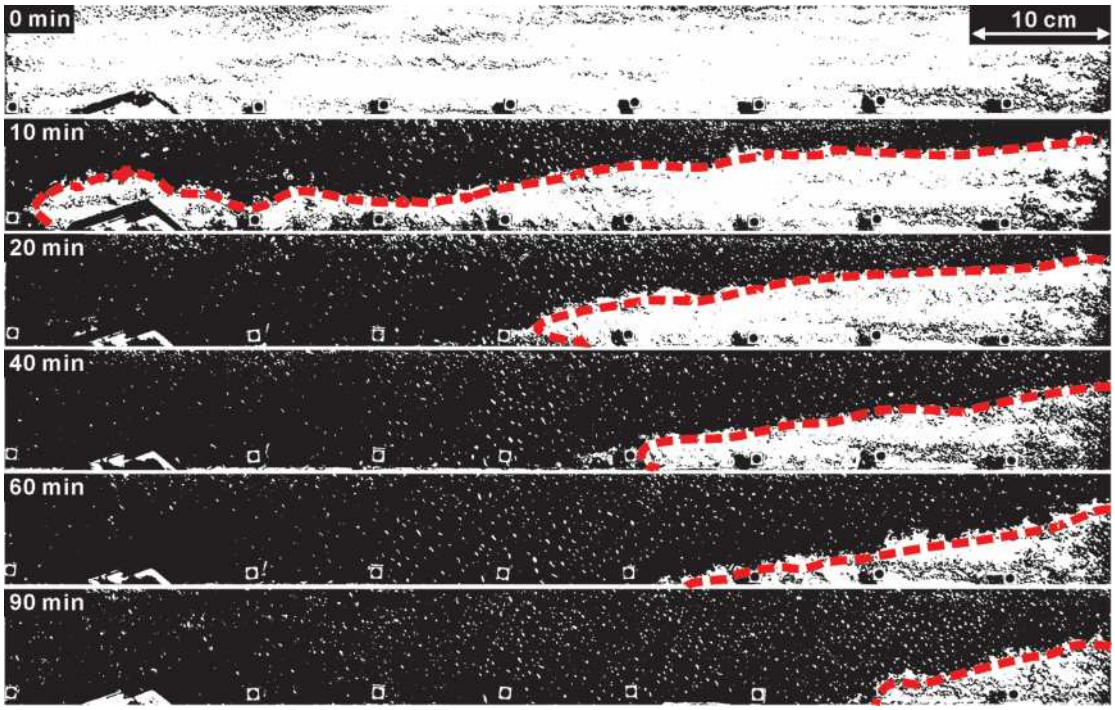

c

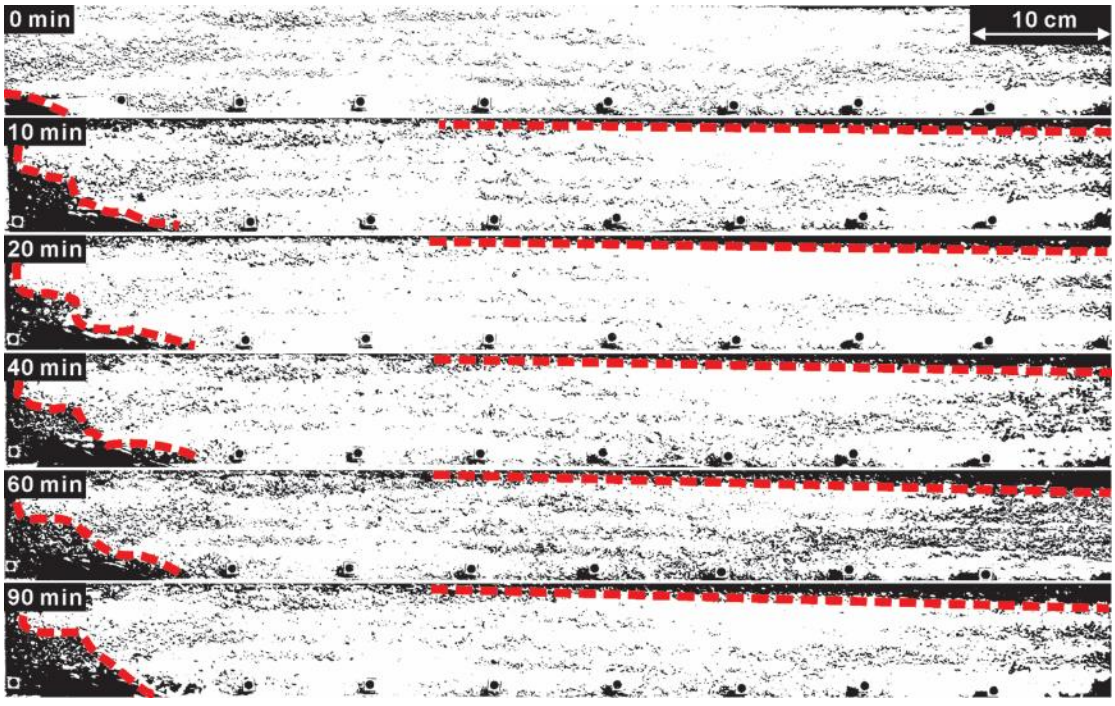

d

Figure 9. Photographs of the infiltration modes, black and white color denote wet and dry zones respectively, dotted red line indicates extent of wetting front (slope toes are at the left-hand side of photos, upper 9 cm of the slope shown). (a) Wettable soil (test 1). (b) Subcritical water repellent soil (test 11). (c) Subcritical water repellent soil (test 8). (d) Water repellent soil (test 3).

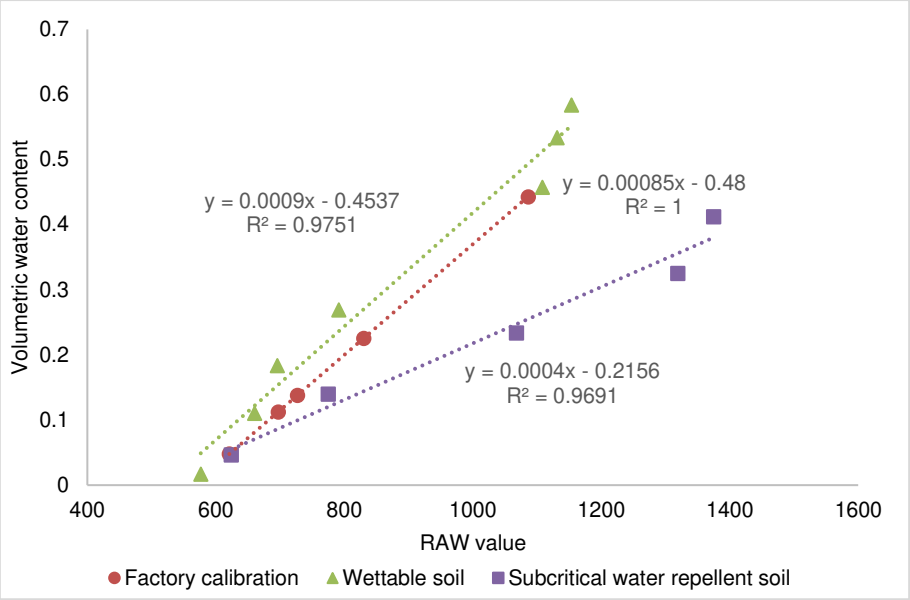

Figure 10: Calibration equations of EC-5 with wettable and subcritical water repellent soils.

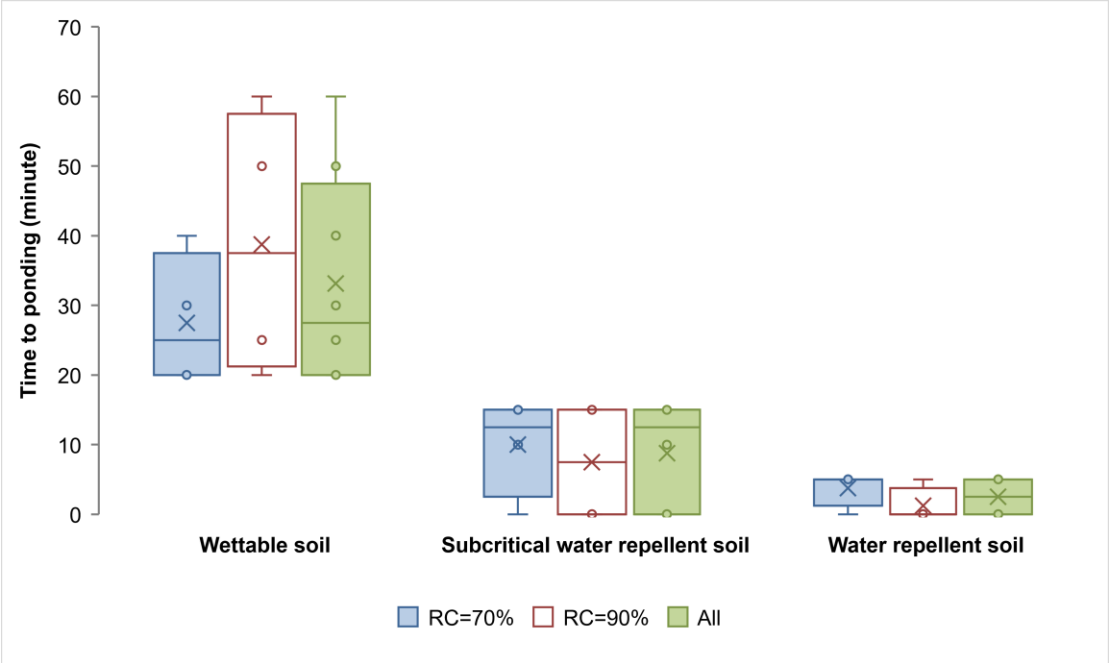
Time to ponding (minute)
70
60
50
40
30
20
10
0
Wettable soil
Subcritical water repellent soil
Water repellent soil
RC=70%
RC=90%
All

a

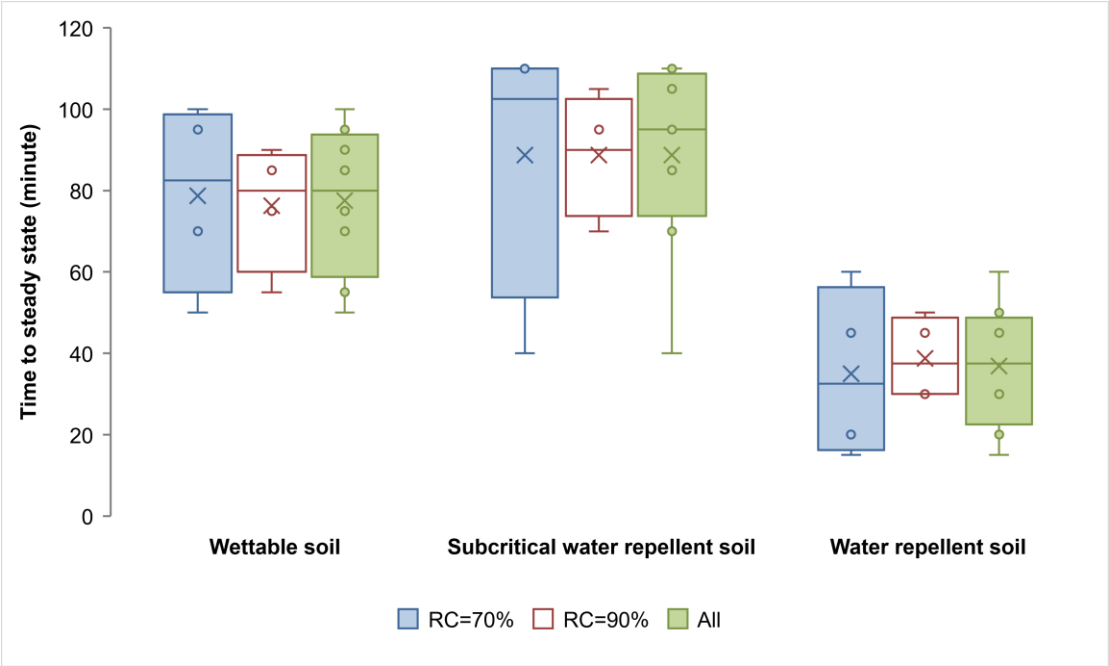
Time to steady state (minute)
120
100
80
60
40
20
0
Wettable soil
Subcritical water repellent soil
Water repellent soil
RC=70%
RC=90%
All

b

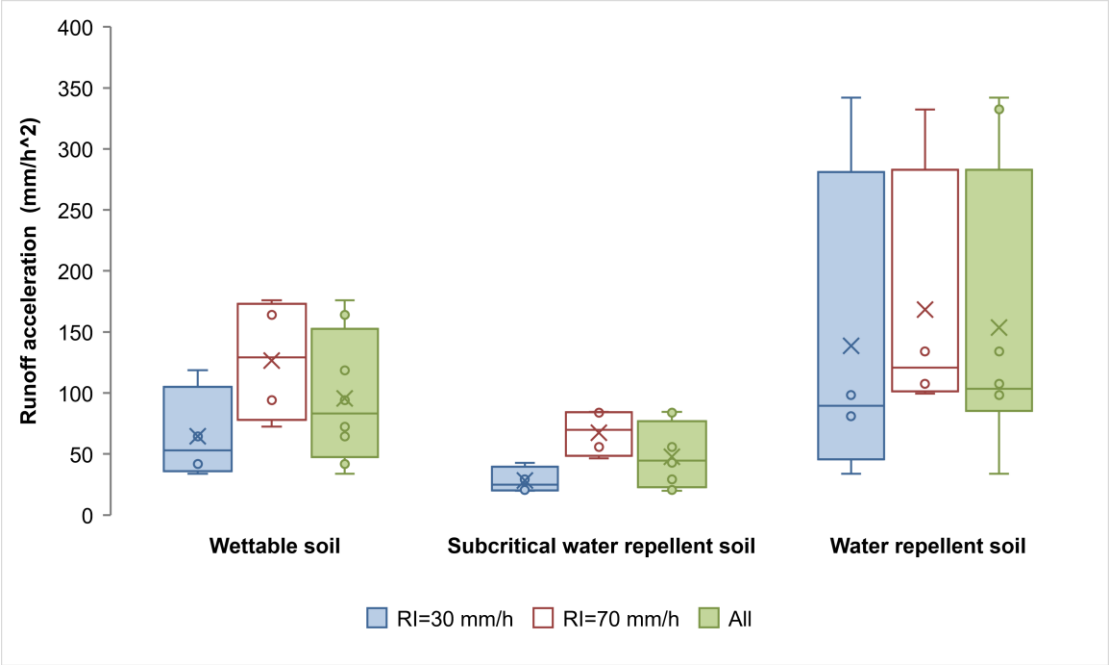
Runoff acceleration (mm/h^2)
400
350
300
250
200
150
100
50
0
Wettable soil
Subcritical water repellent soil
Water repellent soil
RI=30 mm/h
RI=70 mm/h
All

c

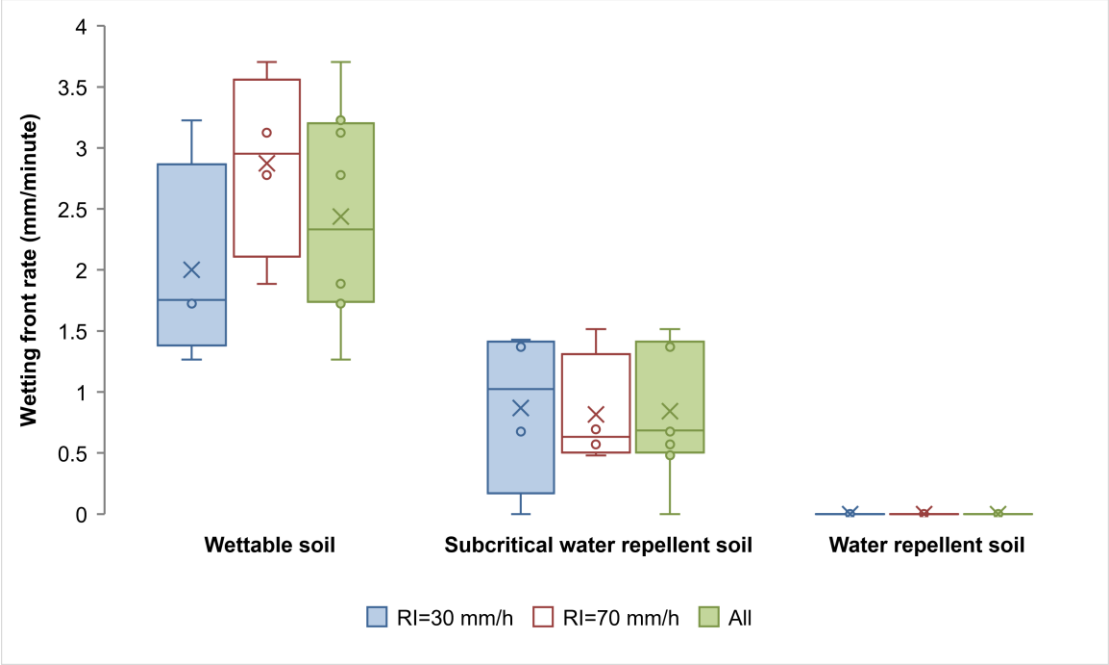
Wetting front rate (mm/minute)
4
3.5
3
2.5
2
1.5
1
0.5
0
Wettable soil
Subcritical water repellent soil
Water repellent soil
RI=30 mm/h
RI=70 mm/h
All

d

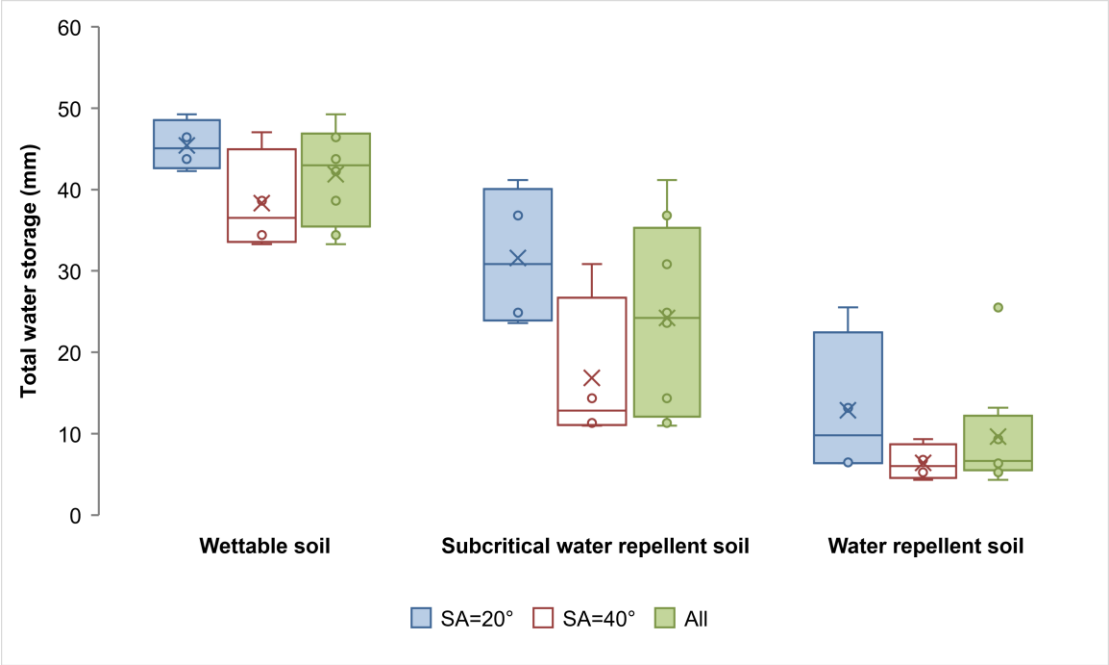

e

Figure 11. Effects of rainfall intensity and slope angle on different soils. (a) Effect of rainfall intensity (RI) on time to ponding. (b) Effect of rainfall intensity (RI) on time to steady state. (c) Effect of rainfall intensity (RI) on runoff acceleration. (d) Effect of rainfall intensity (RI) on wetting front rate. (e) Effect of slope angle (SA) on total water storage.

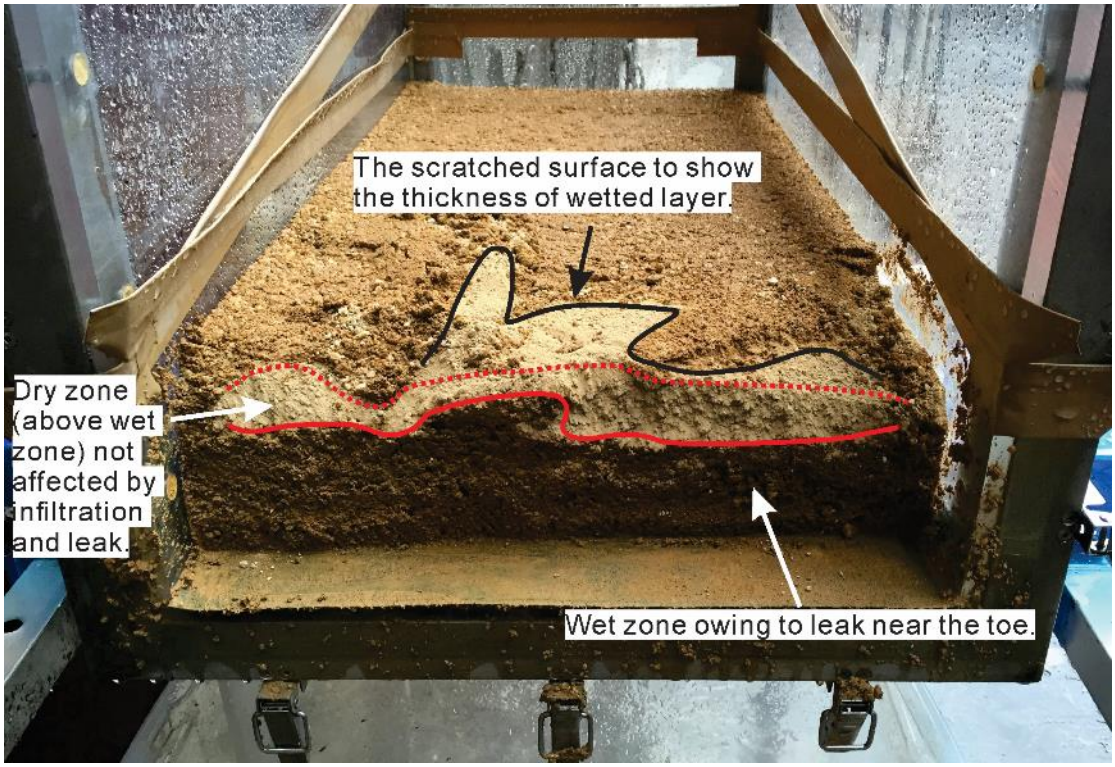

Figure 12. Cross section near the slope toe after test: evidence of leak between the baffle and slope (test 3).

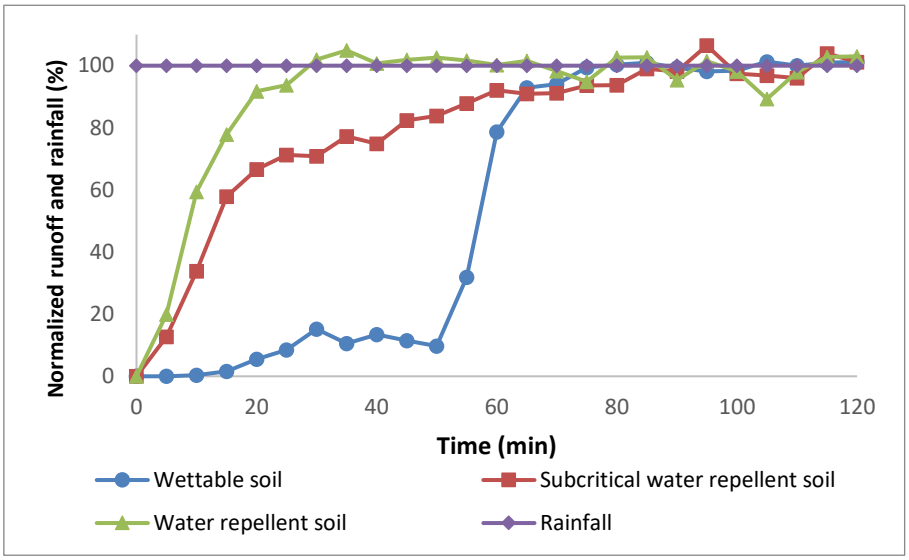

Figure 13. Runoff hydrographs of soils with various wettability (tests 8, 13, 15).